1-1-2013

Geochemical Source Components in Seafloor Lavas in the Aleutian Back-Arc

Max Thomas Siegrist
University of South Carolina - Columbia

Geochemical Source Components in Seafloor Lavas in the Aleutian Back-Arc

by

Max T. Siegrist

Bachelor of Science
Beloit College, 2011

Submitted in Partial Fulfillment of the Requirements

For the Degree of Master of Science in

Geological Sciences

College of Arts and Sciences

University of South Carolina

2013

Accepted by:

Gene Yogodzinski, Director of Thesis

Michael Bizimis, Reader

Scott White, Reader

Lacy Ford, Vice Provost and Dean of Graduate Studies

Abstract

Whole-rock compositions of seafloor lavas are used to constrain the processes and source characteristics contributing to the formation of geochemically distinctive, primitive magma types located in the Aleutian back-arc. Samples were dredged primarily from small volcanic cones on the seafloor, located between the emergent volcanoes and in the back-arc up to 60 km from the volcanic front. Compositions vary from basalt to dacite, with 48-70 % SiO_2 and 4-13 % MgO. Nearly 30% of the samples are primitive, with Mg/Mg+Fe >0.60. Most primitive samples are basalts, which fall into two groups, based on minor and trace element abundances. Low/med-K basalts are similar to primitive basalts throughout the arc with <1 % K_2O and <0.2 % P_2O_5. Most of these contain <500 ppm Sr, <14 ppm Rb, 4-7 ppm La, and La/Yb=3-5. Medium/high-K basalts have higher K_2O and P_2O_5 as well as higher abundances of most incompatible trace elements except Pb (<6 ppm for all primitive basalts). Enrichments are somewhat stronger in the large ion lithophile elements compared to less strongly incompatible elements, resulting in more fractionated trace element patterns in med/high-K basalts (La/Yb=5-10 and Sr/Y=21-39), but without an affect from residual garnet (normalized Dy/Yb=1-2). Strontium and Pb isotopes are generally less radiogenic in med/high-K basalts ($^{87}Sr/^{86}Sr$=0.7028-0.7031, $^{207}Pb/^{204}Pb$=15.49-15.55) compared to low/med-K basalts ($^{87}Sr/^{86}Sr$=0.7030-0.7035, $^{207}Pb/^{204}Pb$=15.53-15.59). The pattern is one of generally less radiogenic Pb and Sr in samples that are more strongly enriched in incompatible elements relative to Pb (K/Pb, Ce/Pb, Hf/Pb). Medium/high-K basalts with

the least radiogenic Sr and Pb have incompatible trace element ratios that approach those of ocean ridge basalts (Ce/Pb=12, Zr/Sm=28, La/Ta=17). The broad isotopic pattern of all Aleutian lavas, and the unradiogenic Sr in med/high-K basalts appear inconsistent with the involvement of an enriched mantle component in the Aleutian back-arc. Paired isotope-incompatible element systematics suggest a stronger influence from depleted mantle in the source that produced the med/high-K basalts. Mixing relationships based on $^{207}Pb/^{204}Pb$ and Ce/Pb indicate a reduced role for subducted sediment, and an increased role for depleted mantle in the source. Higher abundances of K_2O and other incompatible elements in med/high-K basalts appear to require a separate explanation. One possibility is that med/high-K basalts are also produced by significantly lower degrees of partial melting in the mantle, compared to low/med-K basalts.

Table of Contents

List of Figures

Chapter 1

Introduction, Sample Locations, Analytical Methods and Results

1.1 Introduction

Many geochemical studies have concluded that the source of island arc magmas is a mixture of components derived from the sub-arc mantle wedge, subducted sediment and subducted oceanic crust (e.g., Elliott et al., 1997; Hawkesworth et al., 1993; Kay, 1980; Plank and Langmuir, 1993). The nature of these geochemical source components and their role in the formation of subduction magmas, provide an important source of information about the physical conditions present in subduction zones, and about the role of subduction in the evolution of the crust-mantle system.

The Aleutian arc is an ideal setting to investigate geochemical source components because the subduction rate and volume of sediment entering the trench changes along the arc, while the composition and thickness of the arc crust as well as the age of the subducting Pacific plate (50-60 Ma) are effectively constant. Kelemen et al. (2003) emphasized these points and the importance of along-arc changes in subduction rate and sediment flux to the trench, which they argue changes the physical conditions present during magma genesis. They interpreted east-to-west changes in isotopic compositions of Aleutian lavas to reflect a westward decrease in sediment flux to the trench and ultimately to the source of magmas beneath the arc (Kelemen et al., 2003; Yogodzinski et al., 2010; Yogodzinski et al., 1994). Kelemen et al. (2003) noted that oblique convergence results in a lower rate of subduction in the west, increases conductive

cooling of the sub-arc mantle wedge and at the same time increases heating of the subducting plate. Based on these changing physical conditions of subduction, and related east-to-west changes in the compositions of Aleutians lavas, they suggest that subducted basalt plays a stronger role in the source of western Aleutian lavas, because the sub-arc mantle there is expected to be relatively cool, resulting in less contribution from the mantle, compared to the central and eastern parts of the arc.

In this study I present a survey of whole-rock major and trace element compositions, combined with analysis of Sr, Pb, Nd, and Hf isotopes for central and eastern Aleutian seafloor lavas collected by dredging during the 2005 Western Aleutian Volcano Expedition (the WAVE cruise). The focus of this study is on the compositions of seafloor lavas collected between the emergent volcanoes and in back-arc locations up to 60 km from the volcanic front. Almost 30% of lavas from these areas are primitive, with Mg/Mg+Fe >0.60. These primitive samples, which are mostly basalts, provide an outstanding opportunity to evaluate for the first time, cross-arc changes in the source mixture and related processes controlling the compositions of magmas produced in the Aleutian back-arc. An important conclusion of this work is that primitive, back-arc basalts with elevated abundances of K and most incompatible trace elements are produced from a source mixture in which the role of the subducted basalt and sediment is diminished, while that of the sub-arc mantle is enhanced. Isotopic shifts toward unradiogenic Pb in K-enriched back-arc basalts, is consistent with a depleted composition for the Aleutian mantle wedge, and appears to rule out a mantle component beneath the arc similar to nearby plume components.

1.2 Sample Locations

Samples included in this study were taken in 33 dredges collected in locations along more than 1000 km of arc length, from the Kiska Island area in the west to near northern Umnak Island in the east (Fig. 1.1). Dredge targets were primarily volcanic cones and bedrock promontories, located between and behind the much larger emergent volcanoes that define the volcanic front. Many of the cones have smooth and symmetrical shapes, and are clearly the products of constructional volcanic processes (Fig. 1.2a). Others are irregularly shaped and appear to have been subject to significant erosion (Fig. 1.3b). Some of the eroded cones are broad and flat-topped, indicating a history of emergence and erosion to wave base during times of lower sea level (Fig. 1.4c). Several dredges sampled irregularly shaped knobs and bedrock promontories, which we interpret to be eroded and partially buried cones (Fig. 1.5a). One dredge was collected from the submerged flank of the emergent Koniuji volcano.

The smallest cones have base diameters of 0.6-2.1 kilometers and are 120-340 meters high (Fig. 1.2g). The larger cones are 1.4-4.6 kilometers wide at their base and 380-955 meters high (Fig. 1.2f). The largest cones approach the size of small emergent volcanoes such as those in the Islands of Four Mountains (Fig. 1.4), which have base diameters of 4.8-10.5 km and are 888-1,730 meters high.

Many of the dredges are located close to the volcanic front, which we define by straight lines connecting the summits of emergent volcanoes. Dredges in the back-arc are up to 41 km orthogonal distance from the volcanic front, or 60 km from the volcanic front, measured along the direction of Pacific-North America convergence. These locations are 140-206 km orthogonal distances from the plate boundary or 152-309 km

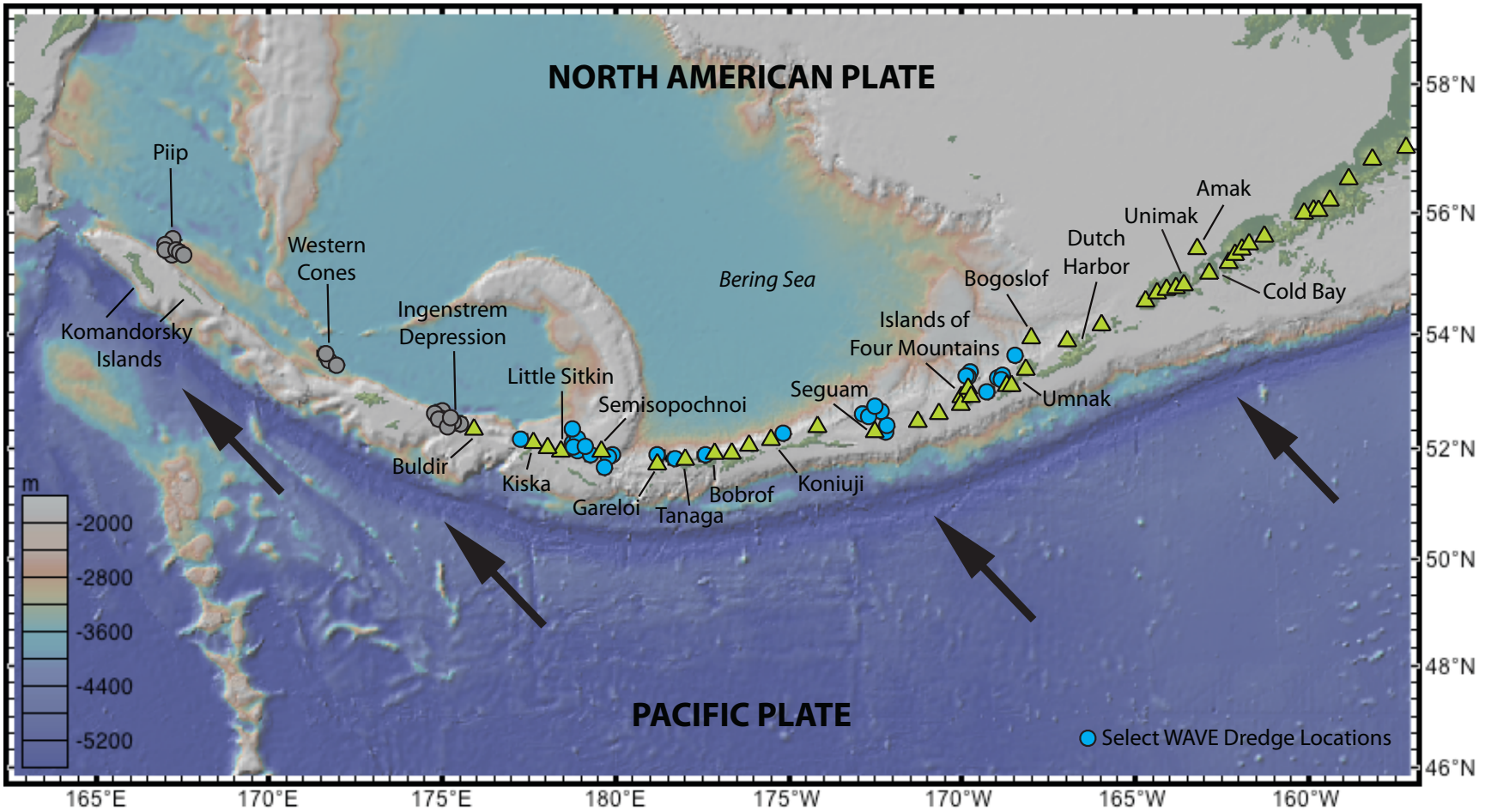

Fig. 1.1. Map illustrating geographical and other features mentioned in this paper. Yellow triangles mark the locations of emergent Aleutian volcanoes. Blue circles represent locations of dredged features analyzed in this study, which were collected during the WAVE cruise. Grey circles mark the locations of dredged features on the western Aleutian seafloor. Black arrows indicate the direction of Pacific-North American convergence along the plate boundary at the Aleutian trench.

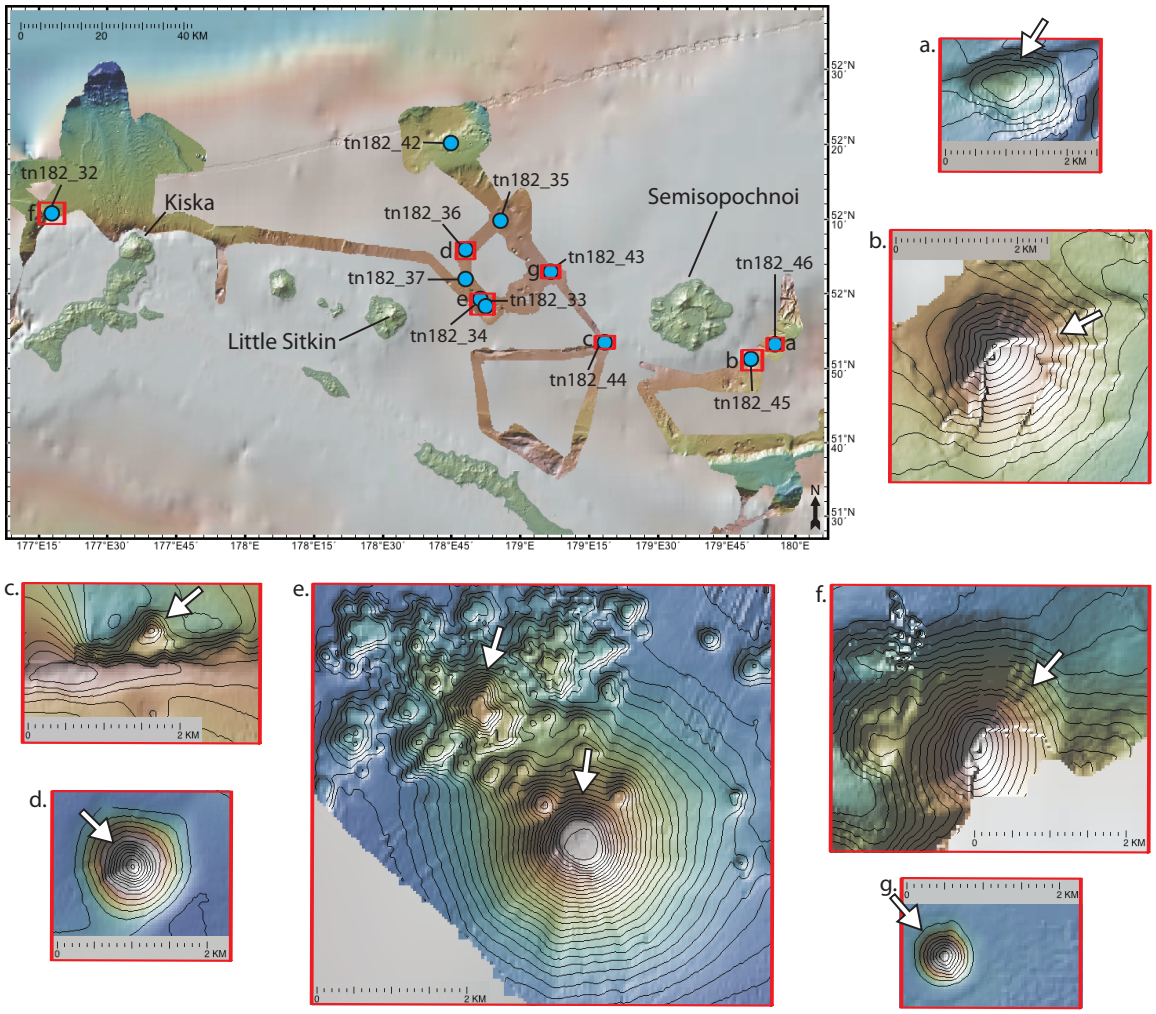

Figure 1.2. Map of the Semisopochnoi, Little Sitkin, and Kiska dredge area with maps illustrating features dredged on the seafloor. Blue circles on the area map indicate locations of dredged features and red extent rectangles correspond to smaller scale maps of dredged features. White arrows on smaller scale maps mark dredge locations and point in the dredge direction. The contour interval is 50 meters for maps b, d and f and 20 meters for maps a, c, e and g. Dredges tn182_35, tn182_37 and tn182_42 sampled symmetrical cones similar to tn182_36 and tn182_43, illustrated in maps d and g respectively.

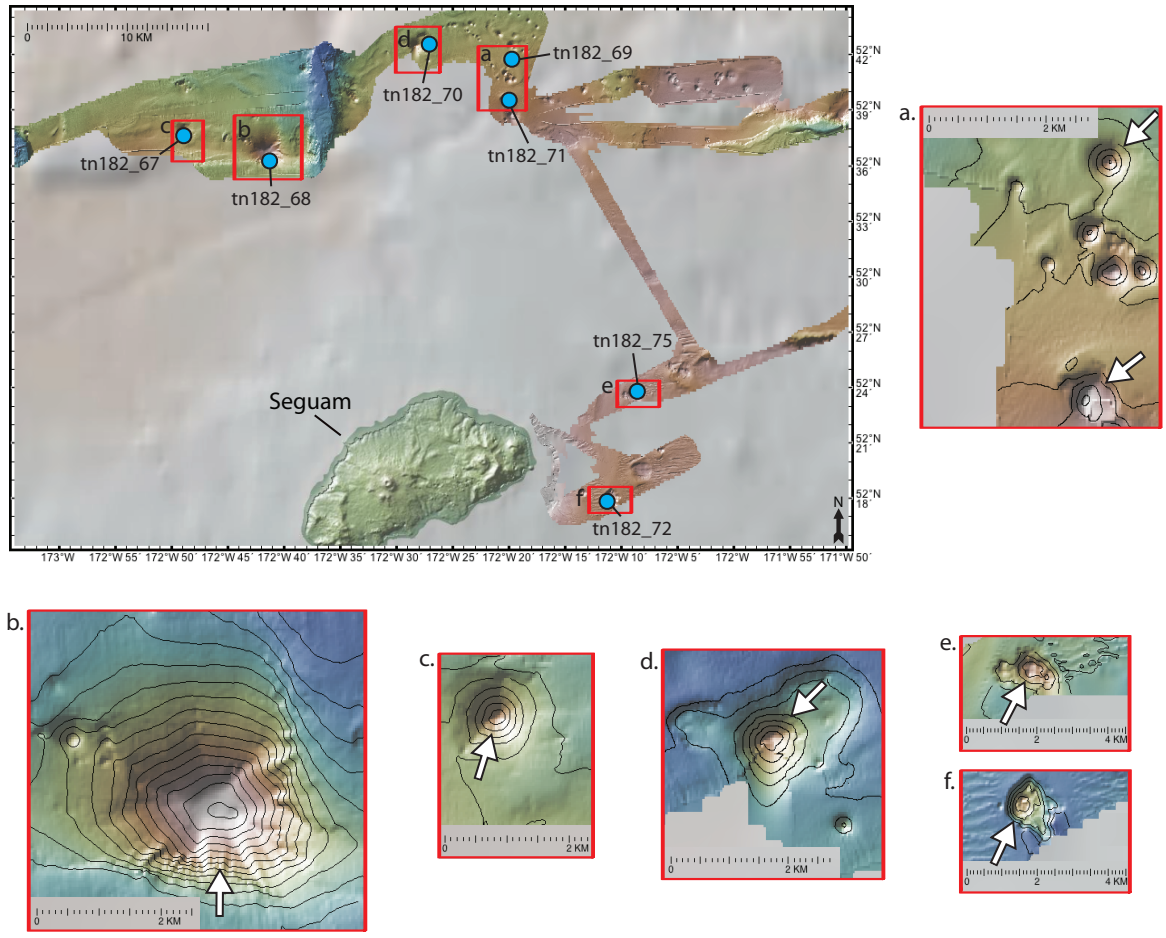

Figure 1.3. Map of the Seguam dredge area with maps illustrating features dredged on the seafloor. Symbols are as in Fig. 1.2. The contour interval is 50 meters for maps a-f.

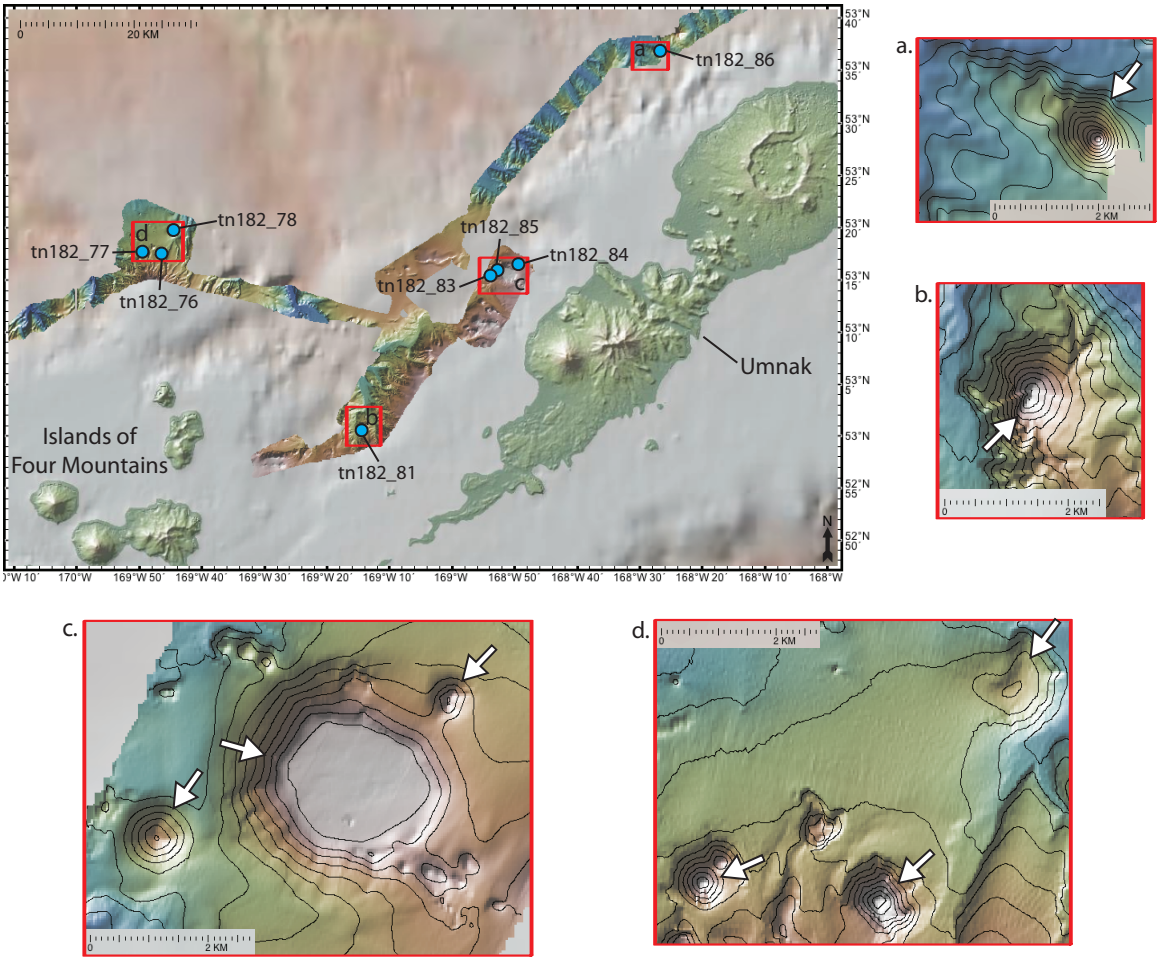

Figure 1.4. Map of the Umnak and Island of Four Mountains dredge area with maps illustrating features dredged on the seafloor. Symbols are as in Fig. 1.2. The contour interval for maps a-d is 50 meters.

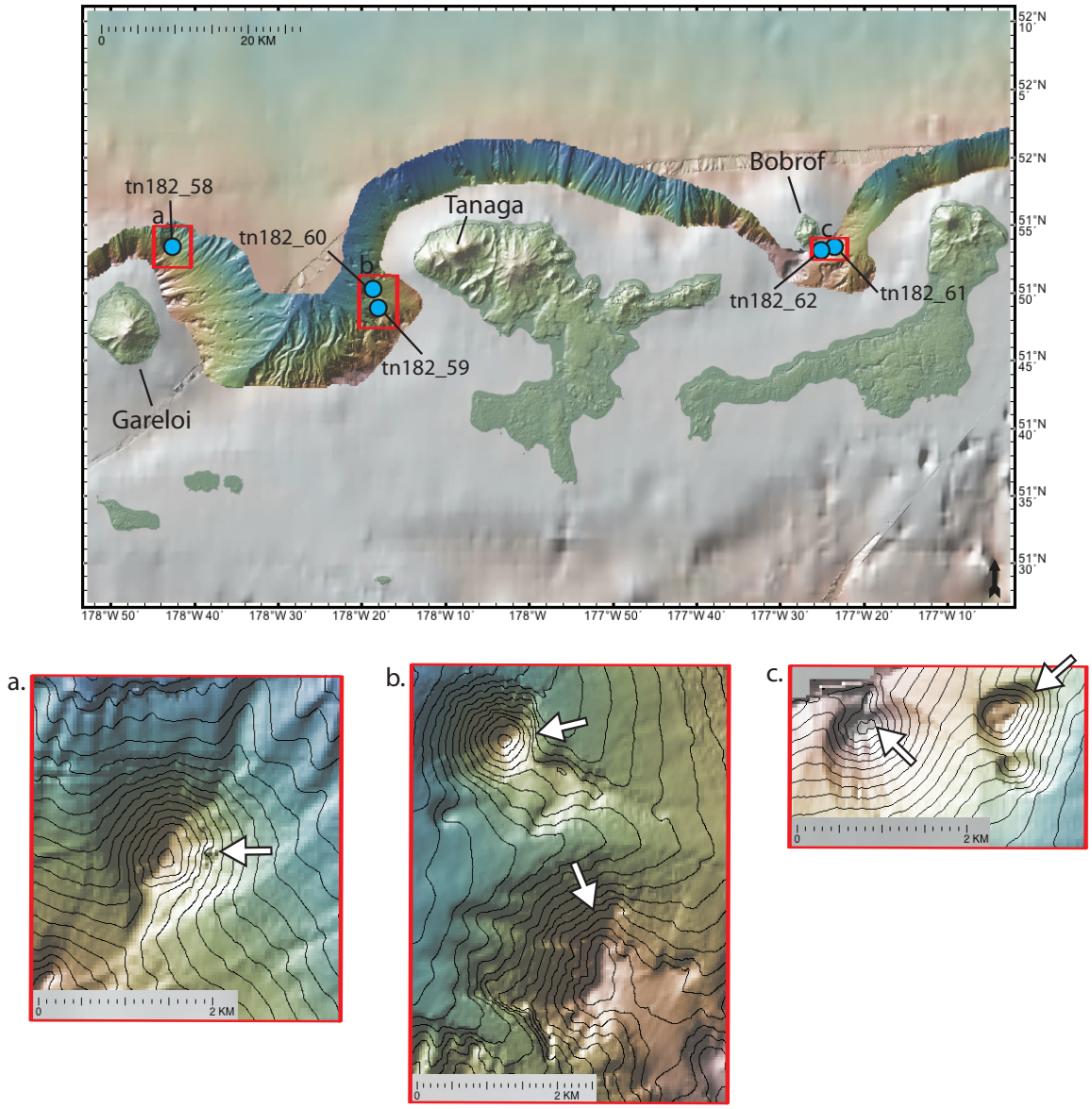

Figure 1.5. Map of the Bobrof, Tanaga and Gareloi dredge area with maps illustrating features dredged on the seafloor. Symbols are as in Fig. 1.2. The contour interval is 50 meters for maps a-c.

measured from the plate boundary along the direction of Pacific-North America convergence.

Samples included in the study appear fresh in hand sample and were free of significant Mn-oxide or other mineral coatings or significant signs of alteration or weathering. Samples dredged from bedrock promontories located more than approximately 10 km south of the volcanic front in the Amchitka, Semisopochnoi and Gareloi survey areas (Fig. 1.1), were excluded from this study because their ages are uncertain (they could be several million years old) and because they probably formed at a time when the Aleutian volcanic front was located well south of its present location. Radiometric dating indicates that samples dredged from deep bedrock structures, such as submarine canyons, are Eocene to early Miocene in age, (Jicha et al., 2005). These samples, which were produced during an early phase of Aleutian arc growth, show significant signs of alteration and weathering, and have also been excluded from this study.

1.3 Analytical Methods

Rock samples were broken to 16-18 g of coarse fragments with a hammer, and reduced to 2-3 mm-size chips with a jaw crusher. The rock chips were then rinsed with distilled water and dried. The dried chips were ground to a powder in an agate container for 30 minutes, using a *Fritsch* planetary ball mill.

Preparation of whole-rock samples for x-ray fluorescence (XRF) analysis was done at the University of South Carolina following the procedures of Johnson et al. (1999). Glass disks were made from a mixture of 3.5 g of rock powder and 7 g of Li-tetraborate flux. The rock-flux mixtures were fused in graphite crucibles at 1050° C for

10 minutes and quenched in graphite molds. The samples were then re-ground in a *RockLabs* bench top ring mill in a tungsten-carbide container. The resultant powders were then fused and quenched in graphite for a second time. One surface of each glass disk was then flattened on a diamond lap. Final finishing of the flattened surface and analysis by XRF were done at the Washington State Geoanalytical Lab in Pullman, WA. The XRF data are reported on an anhydrous basis with major element totals recalculated to 100%.

Digestion of samples for whole-rock trace element analysis by ICPMS was adapted from the hydrothermal decomposition method of Krogh (1973). Approximately 40 mg of rock powder was weighed into 3 mL teflon capsules. The capsules, with their lids placed loosely on them, were then positioned in teflon inserts of steel digestion bombs (Parr #4745) containing 4-5 mL of a 3:1 mixture of HF:HNO_3. The steel bombs were then assembled and placed in the oven at 150° C for 4-5 days. After removing the bombs from the oven, the digested samples were transferred to 15 mL teflon capsules using 4-6 mL of 15N HNO_3. The samples were then placed on a hotplate at approximately 90° C and evaporated to insipient dryness. Dissolution in 4-6 mL of 15N HNO_3 and evaporation to incipient dryness was repeated twice more. Samples were then heated gently overnight in 6 mL of a 4:1 mixture of 18 MΩ H_2O and 15N HNO_3. Most solutions are clear and free of precipitates after this step. Additional dissolution/drying steps in 15N HNO_3 were necessary to produce clear solutions for only a small number of samples.

Solutions produced by the digestion method described above were transferred to HDPE bottles and diluted 2000 times the initial powder weight with de-ionized water

containing 25 ppb In and 1% HNO_3 by volume. The final result was an 80 mL solution with 2.5% HNO_3 containing 500 ppm of dissolved rock and 25 ppb of In, which is used as an internal standard.

Abundances of 26 trace elements were measured at the University of South Carolina on a *Varian* 820-MS quadrupole ICP-MS. Blank solutions were measured at the beginning and end of each analytical run. Unknown solutions were bracketed by the AGV-1 reference standard, which was analyzed after every five unknown samples throughout each run. Indium-normalized and blank-corrected count rates for unknowns were quantified against the AGV-1 standard, using reference values from Kelley et al. (2003) and from the online GeoRem database. Additional USGS rock standards were run periodically to evaluate precision and accuracy.

For Nd and Sr isotopes, approximately 100 mg of rock powder was leached with 6 N HCl in a sealed, teflon capsule at ~120° C for one hour. The resulting leachate was decanted and samples were rinsed three times with 18 MΩ H_2O. The leached samples were then digested in 4 mL of an HF:HNO_3 mixture (3:1). Precipitates were removed from the solutions using the steps described above for trace element sample digestion. Samples were then dissolved in 2.5 N HCl and centrifuged for 10 minutes at 40,000 rpm. The centrifuged samples were loaded onto a ~5 mL bed of cation-exchange resin (200-400 μm Eichrom 50W-X8) in teflon columns. Light rare-earth element and Sr fractions were separated from the rock matrix with elutions in 6 N and 2.5 N HCl respectfully. Strontium fractions were dried, dissolved in 0.001 N HNO_3 and loaded on an Eichrom SR-B50-S resin in teflon micro-columns. The samples were rinsed with 3.5 N HNO_3 and separated from the resin with 0.001 N HNO_3. Light rare-earth element fractions were also

dried and dissolved in 0.25 N HCl. These were loaded on Eichrom LN-B25-S resin in teflon micro-columns. Neodymium fractions were separated from other light rare-earth elements with 0.25 N HCl.

For Pb isotopes, hand-picked rock chips were rinsed in de-ionized water, sonicated and dried. The cleaned chips were then leached with 6 N HCl in a sealed, teflon capsule at ~120° C for one hour. The resulting leachate was decanted and the samples were rinsed three times with 18 MΩ H_2O. The leached rock chips were then digested in ~6 mL of an HF:HNO_3 mixture (3:1) on a hotplate at ~90° C for 24 hours. The digested samples were then dissolved in ~1 mL of 2 N HBr and evaporated to dryness at ~90°C on a hotplate. This step was repeated twice more. The samples were then placed on BioRad AG-1 X8 anion-exchange resin in teflon micro-columns. The Pb fraction was removed from the rock matrix by the addition of two separate mixtures of 2.5 N HNO_3 and 2 N HBr to the column (2:1 and 2:0.15). The eluted Pb fractions were passed through the columns a second time using the same steps for additional cleaning.

Isotope ratios were measured on the Thermo Fisher Neptune in the Center for Elemental Mass Spectrometry at the University of South Carolina. The Sr and Nd results were normalized to $^{86}Sr/^{88}Sr=0.1194$ and $^{146}Nd/^{144}Nd=0.7219$, assuming exponential fractionation behavior. Seventeen measurements of the SRM987 Sr isotope standard returned an average of 0.710254 for $^{87}Sr/^{86}Sr$ ($2\sigma= 0.000030$). Results are corrected against a value for $^{87}Sr/^{86}Sr$ in SRM981 of 0.10248. Four measurements of the Jndi Nd isotope standard returned an average of 0.512096 for $^{143}Nd/^{144}Nd$ ($2\sigma= 0.000015$). Three measurements of the La Jolla Nd isotope standard returned an average of 0.511840 for $^{143}Nd/^{144}Nd$ ($2\sigma= 0.000011$). Results were corrected against a reference value of

0.512115 for Jndi. Lead isotope samples were spiked with thallium to monitor in-run mass fractionation of Pb isotopes (White et al., 2000). Thirteen analyses of the NBS981 standard measured by this method produced values for $^{206}Pb/^{204}Pb$=16.921, $^{207}Pb/^{204}Pb$=15.470, and $^{208}Pb/^{204}Pb$=36.630. Results for Pb isotopes were corrected against accepted values for NBS981 from Todt et al. (1996 - $^{206}Pb/^{204}Pb$=16.936, $^{207}Pb/^{204}Pb$=15.489, and $^{208}Pb/^{204}Pb$=36.701).

1.4 Results

The 159 samples of central and eastern Aleutian seafloor lavas analyzed for this study span a wide range of major element compositions, from basalt to dacite, with 48-70 % SiO_2 (Fig. 1.6). Most samples are basalts (88), with a smaller number of basaltic-andesites (22), andesites (37) and only a few dacites (12). The seafloor lavas fall primarily in the medium-K field (Fig. 1.6C), which is typical for Aleutian and other island-arc volcanic rocks worldwide (Gill, 1981). The Aleutian seafloor lavas also span a wide range FeO*-MgO-SiO_2 compositions and so display both tholeiitic and calc-alkaline igneous series characteristics (Fig. 1.6G).

A significant number of the seafloor lavas are primitive basalts which contain more than 8 % MgO and have molar Mg/Mg+Fe greater than 0.60 (Mg#>0.60 – Fig. 1.6D). Many of these samples have medium–low K_2O contents (0.5-1.0 %, Fig. 1.6C-D), which are typical for primitive and least-evolved Aleutian basalts (Gust and Perfit, 1987; Kay and Kay, 1994; Nye and Reid, 1986). The seafloor lavas include a second group of basalts that are similarly primitive (8-11 % MgO, Mg#>0.60) but contain higher K_2O (1.0-1.3 %). These higher-K basalts, which fall around the med/high-K boundary line in Fig. 1.6C, also have higher TiO_2 (1.0-1.6 %, Fig. 1.6A-B) and P_2O_5 (0.23-0.45 %, Fig.

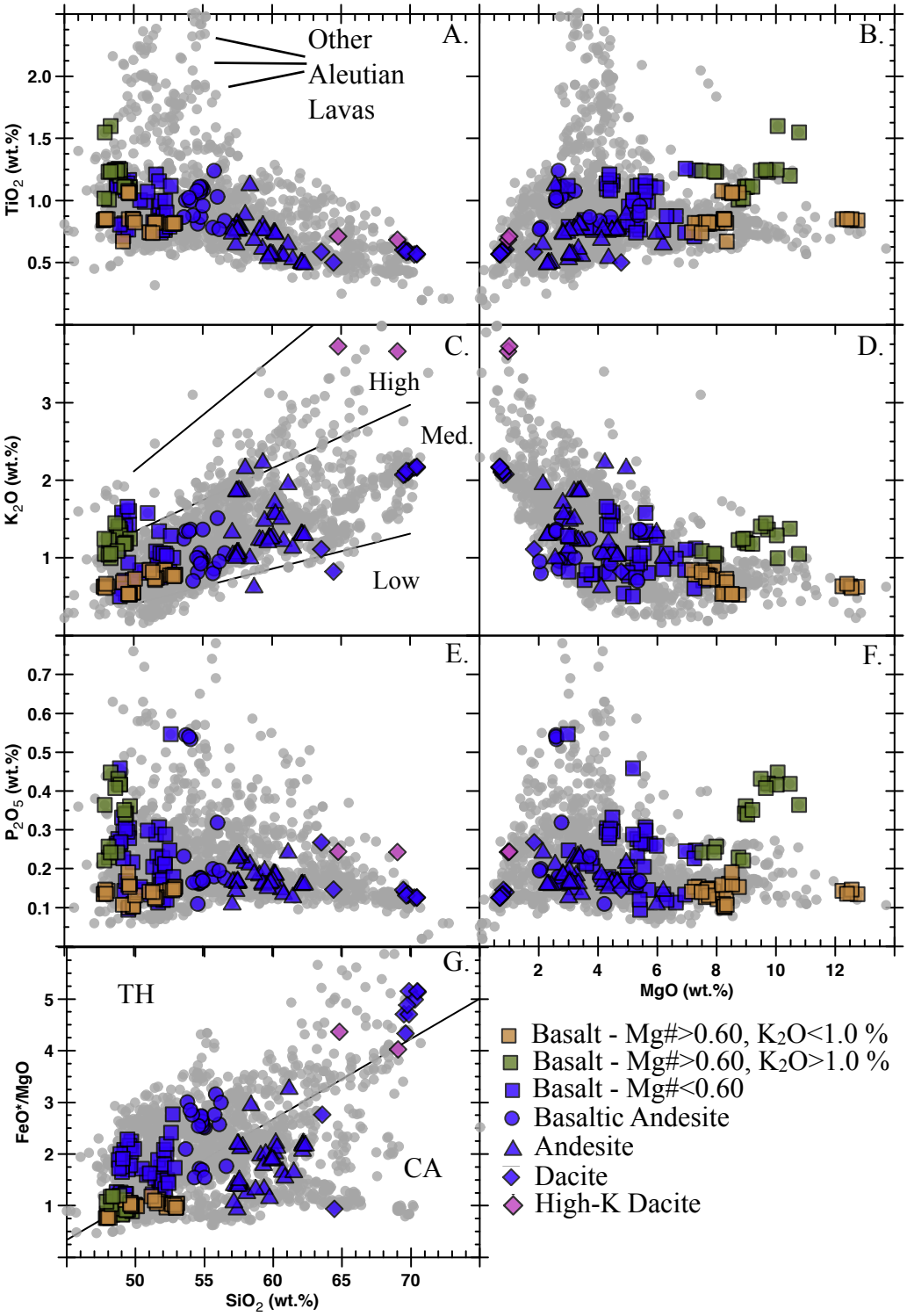

Figure 1.6. Harker and Fenner diagrams of TiO_2, K_2O, and P_2O_5 as well as a FeO*/MgO Harker diagram of central and eastern Aleutian seafloor lavas plotted with other Aleutian lavas (grey circles). Other symbols are as indicated in the legend. Black lines on the K_2O Harker diagram represent the boundaries of the low, medium, and high-K fields, and are after Gill (1981). The black line on the FeO*/MgO Harker diagram separates tholeiitic (TH) from calc-alkaline (CA) rocks and is after Miyashiro (1974).

1.6E-F) compared to the low/med-K basalts (TiO_2=0.67-1.1 %, P_2O_5=0.10-0.20 %), which again, are more typical of primitive basalts throughout the Aleutians (Fig. 1.6).

Incompatible trace elements are also clearly different in the low/med-K and med/high-K basalt types. This is illustrated in Fig. 1.7A which shows that the med/high-K basalts have generally higher abundances for all rare-earth elements (REEs). In this way these basalts appear similar to basalts and andesites from Amak and Bogoslof, which are the two large, emergent volcanoes that lie well behind the Aleutian volcanic front (Fig. 1.7B). Figure 1.8 shows that except for Pb, the med/high-K basalts have generally higher abundances of all incompatible elements. The med/high-K basalts are also more strongly enriched in the light REEs (higher La/Yb) but have ratios of middle to heavy REEs (Dy/Yb) similar to those of the low/med-K basalts (Fig. 1.7A, 1.8). Abundances of the middle and heavy REEs (Dy to Y on Fig. 1.8) in all of the primitive seafloor basalts discussed here are below those of MORB (Fig. 1.8). Finally, it is evident that although the med/high-K basalts are relatively Ti-rich, the depletion of Ta-Nb and Hf-Zr relative to similarly incompatible REEs persists, even for basalts with >1.5 % TiO_2 and 14-15 ppm Nb (Fig. 1.8).

Petrographic observations also illustrate some differences in the primitive basalt groups. Olivine up to 2-3 mm in long dimension is the only phenocryst phase present in three med/high-K basalt samples studied (dredges 35-37 – Fig. 1.9). These samples also have similar groundmass texture/mineralogy where they are vesicular and contain olivine, plagioclase, opaques and glass. Observations of thin sections for six of the low/med-K primitive basalts illustrate a range of phenocryst types, from olivine only (dredge 84), to olivine and plagioclase (dredge 43), to olivine and clinopyroxene (dredge

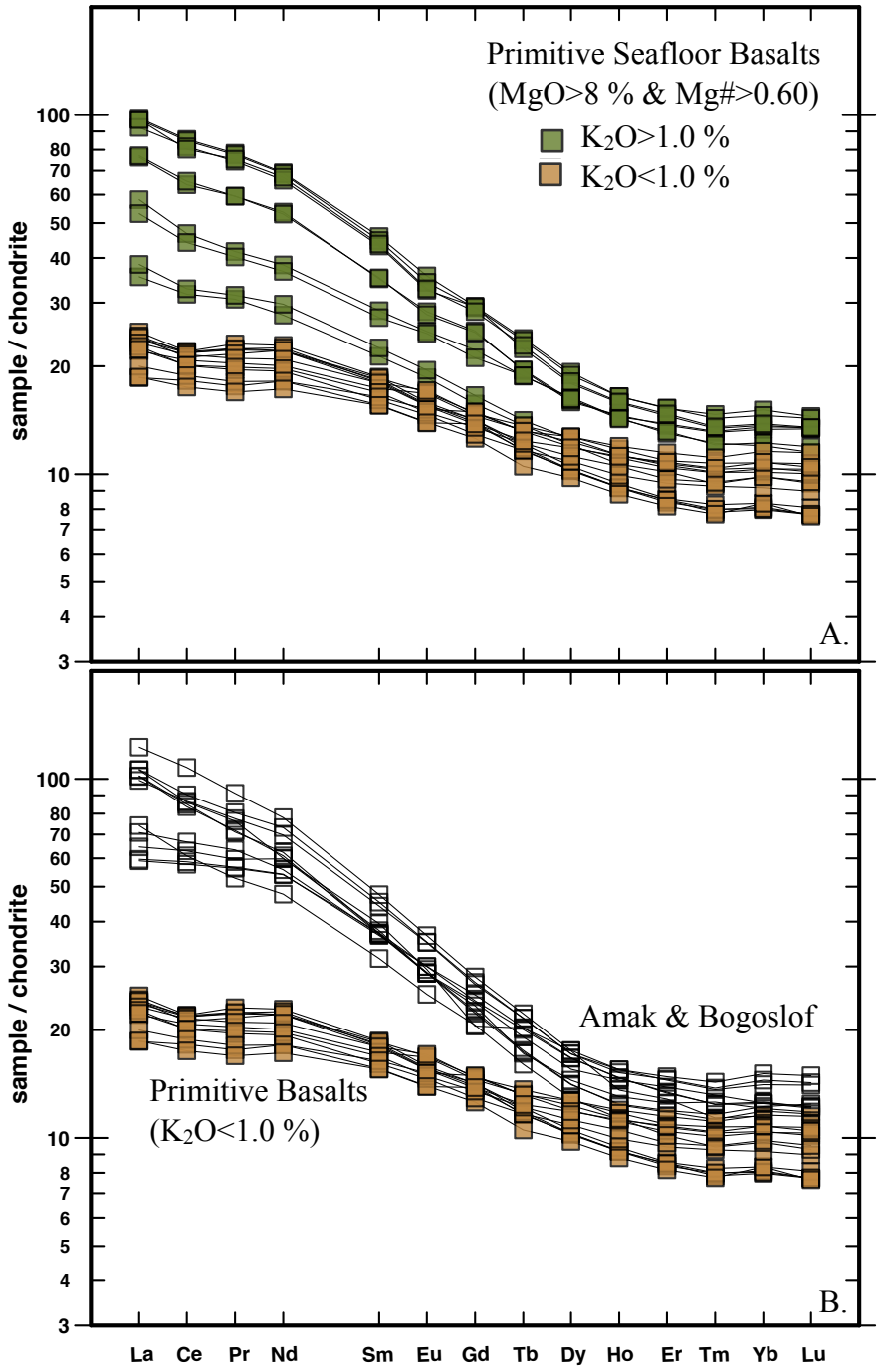

Figure 1.7. Chondrite-normalized rare-earth element abundances for primitive (MgO>8 % and Mg#'s>0.60) seafloor basalts (A) and lavas from Amak and Bogoslof (B). Amber squares are low/med-K primitive basalts with K_2O<1.0 % and green squares are med/high-K primitive basalts with K_2O>1.0 %. Amak and Bogoslof are two emergent volcanoes in the Aleutian back-arc and are represented by white squares. Normalizing values are from McDonough and Sun (1995).

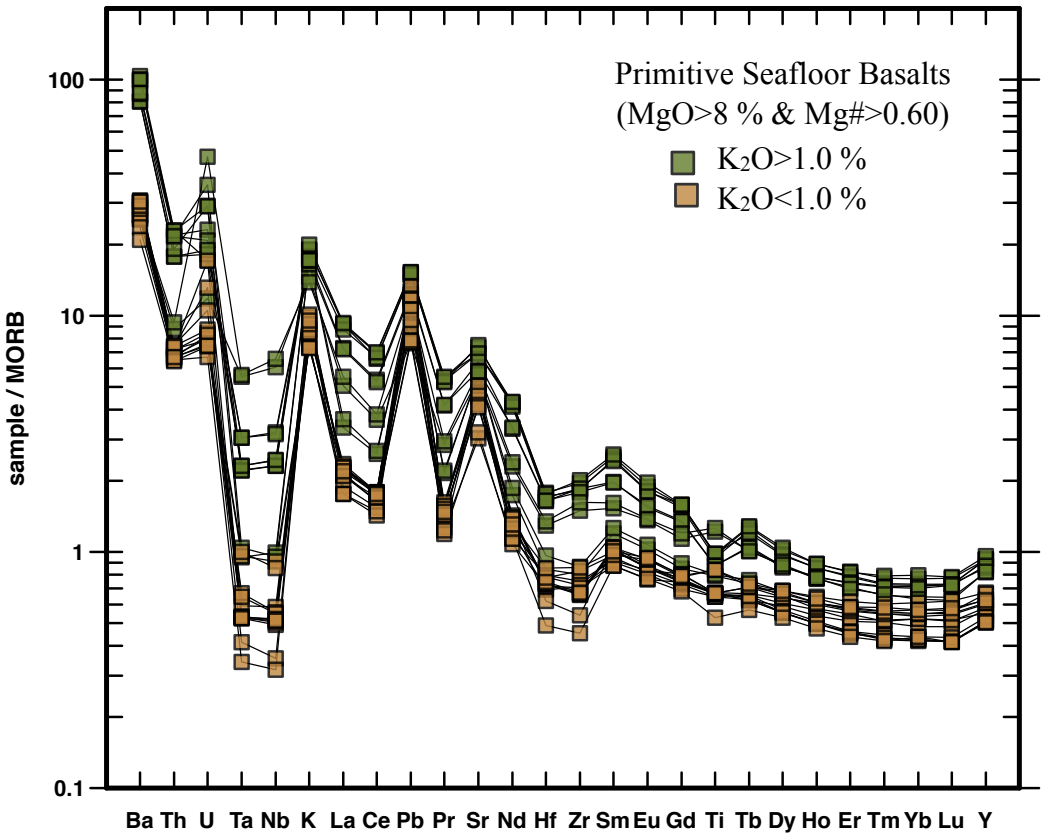

Figure 1.8. MORB-normalized incompatible element abundances for primitive seafloor basalts. Symbols are as in Fig. 1.7A. Normalizing values are from Sun and McDonough (1989).

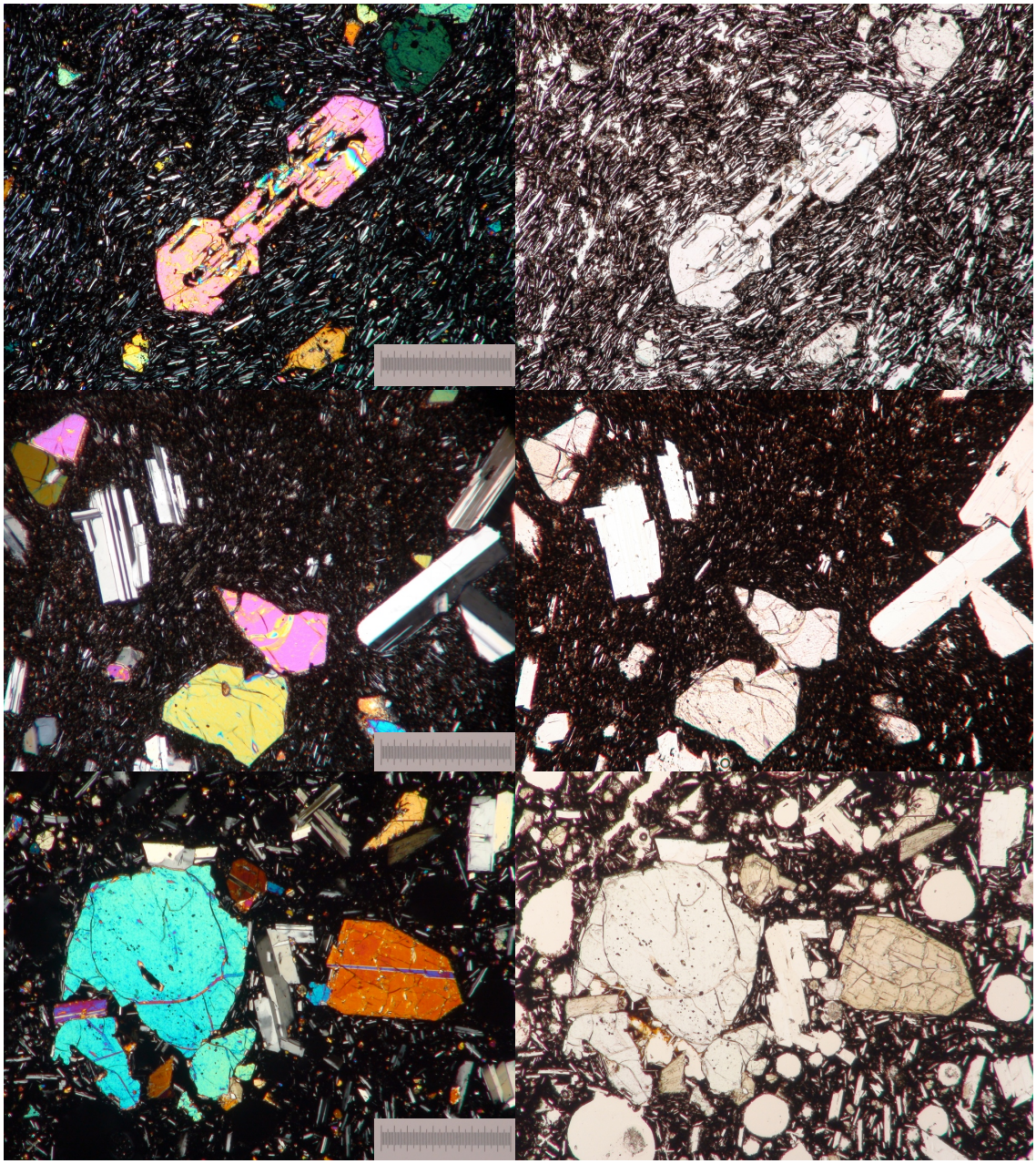

Figure 1.9. Photomicrographs of high MgO basalts showing different phenocryst assemblages; olivine, olivine and plagioclase, and olivine, plagioclase, and clinopyroxene. Scale bar in each photomicrograph is one millimeter.

77), to dominantly olivine with sparse microphenocrysts of clinopyroxene and small plagioclase-pyroxene glomerocrysts (dredge 69), and to olivine, plagioclase and clinopyroxene (dredges 67 and 75).

The seafloor basaltic andesites have Mg#s mostly <0.60 and fall primarily in the tholeiitic field, whereas the andesites have on average, similar or higher Mg#s, and so fall predominantly in the calc-alkaline field (Fig. 1.6G). Abundances of TiO_2, P_2O_5, K_2O and other major elements in most of the basaltic andesites and andesites are typical of those in Aleutian lavas at intermediate silica (Fig. 1.6, 1.10). Basaltic andesite REE patterns are similar to those in the low/med-K basalts, but at somewhat higher average abundances (Fig. 1.11). Some basaltic andesites have more fractionated REEs (higher La/Yb) and so appear more similar to the med/high-K basalts (compare Figs. 1.11A and 1.7A). Most of the andesites have elevated REE abundances, similar to the basaltic andesites, but with more pronounced negative Eu anomalies (Fig. 1.11B). Some andesites also have more fractionated REE patterns (higher La/Yb) resulting from relatively low abundances of middle and heavy REEs, similar to those in the low/med-K basalts (Fig. 1.11B).

Several of the basaltic andesites and andesites have unusually high Sr compared to average Aleutian lavas at intermediate silica (>700 ppm, Fig. 1.12A). Some of these have distinctive trace element patterns, with high light REEs (La>50X chondrites), low Y and heavy REEs (<7X chondritic – Fig. 1.11C) and strong fractionation between the middle and light REEs (high Dy/Yb). These high-Sr andesites also have elevated Ta and Nb, which result in low La/Ta and La/Nb ratios similar to those of MORB (Fig. 1.13). Abundances of Hf and Zr in the high-Sr andesites are also relatively high, especially compared to Sm (Fig. 1.13).

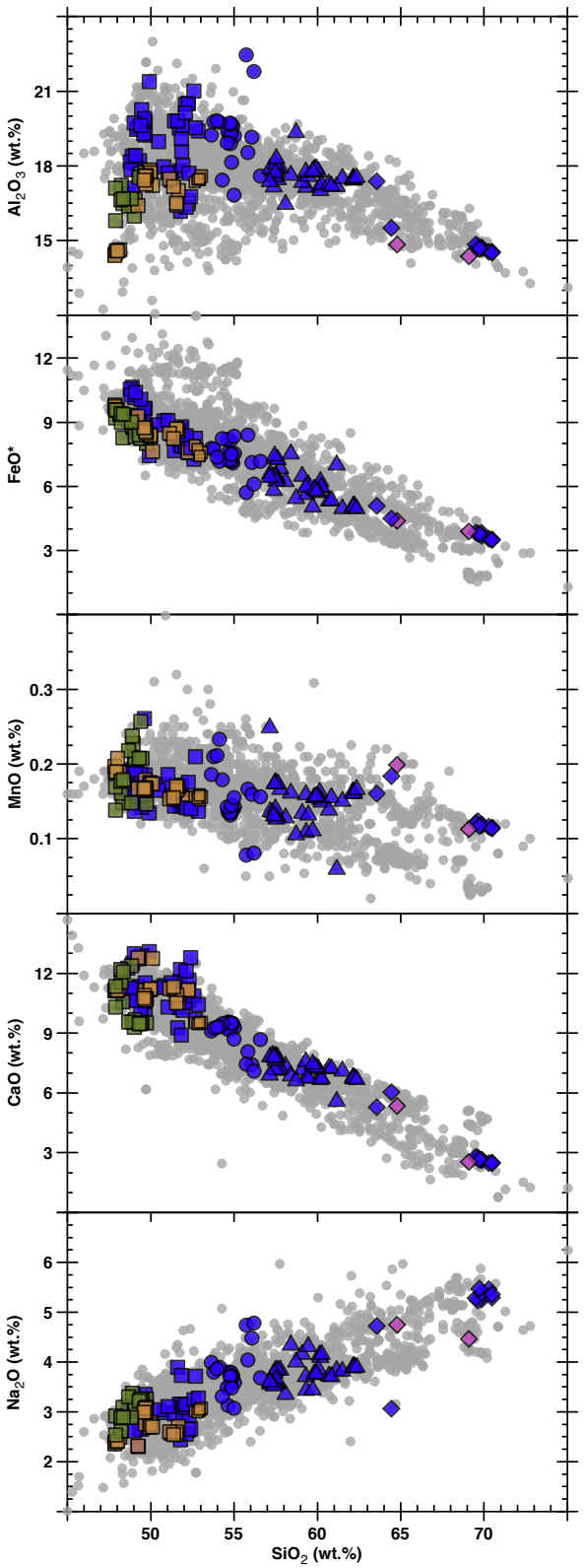

Figure 1.10. Harker diagrams of Al_2O_3, FeO*, MnO, CaO and Na_2O. Symbols are as in Fig. 1.6.

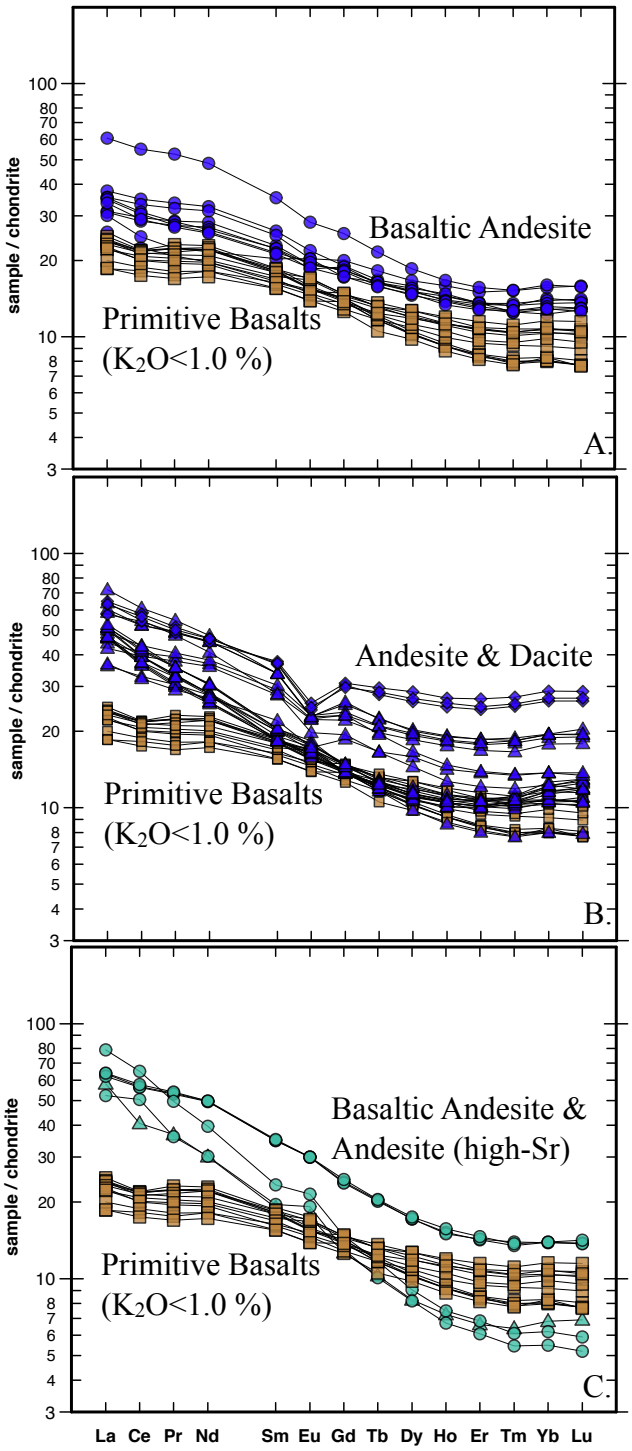

Figure 1.11. Chondrite-normalized rare-earth element abundances for seafloor basaltic andesites, andesites and dacites. Amber squares are as in Fig. 1.7. Other symbols in 1.11A and 1.11B are as in Fig. 1.6. Teal circles and triangles in 1.11C represent high-Sr (>700 ppm) basaltic andesites and andesite, respectfully. Normalizing values are from McDonough and Sun (1995).

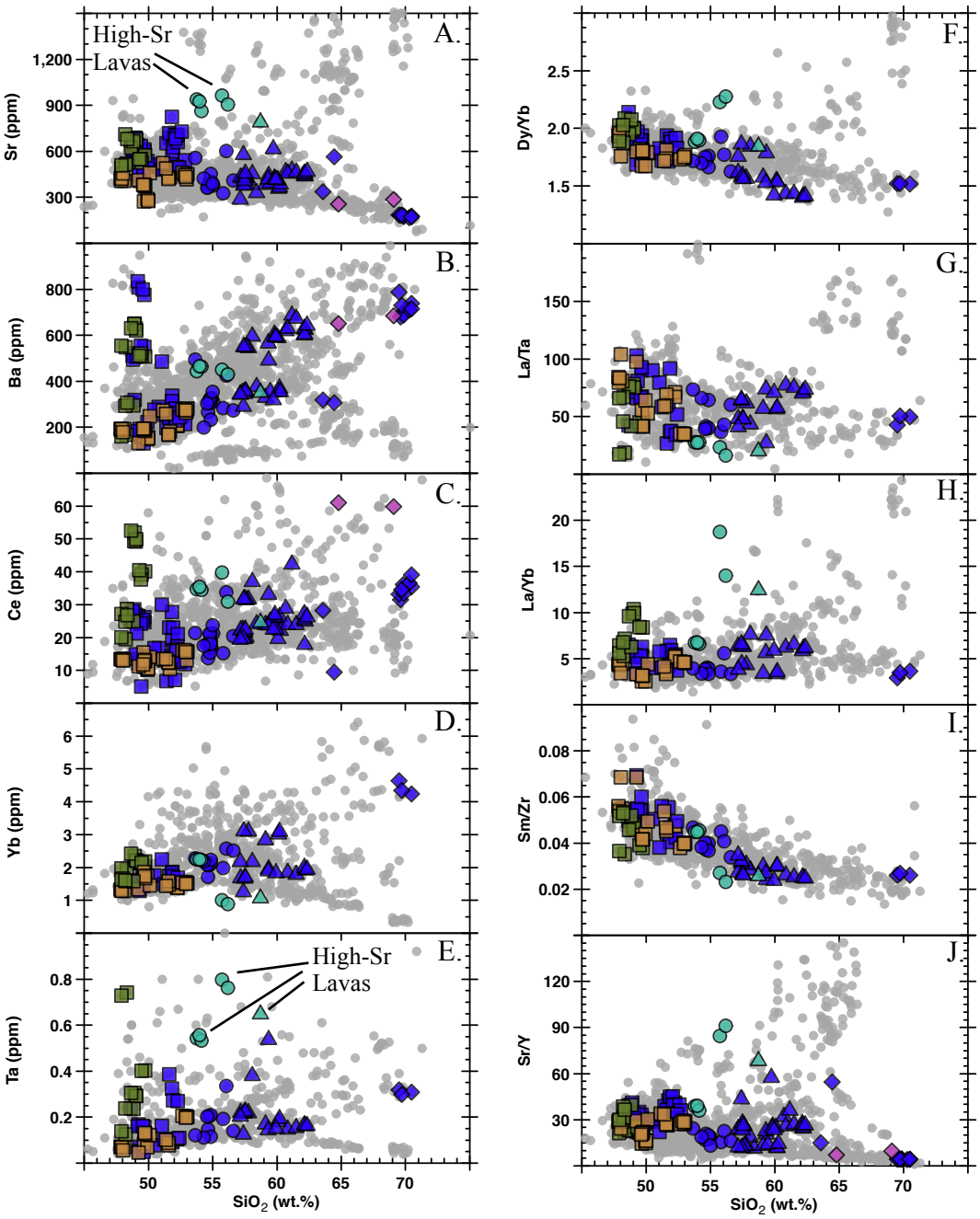

Figure 1.12. Harker diagrams of key incompatible trace element abundances and incompatible trace element ratios. Teal circles and triangles are high-Sr lavas and other symbols are as in Fig. 1.6.

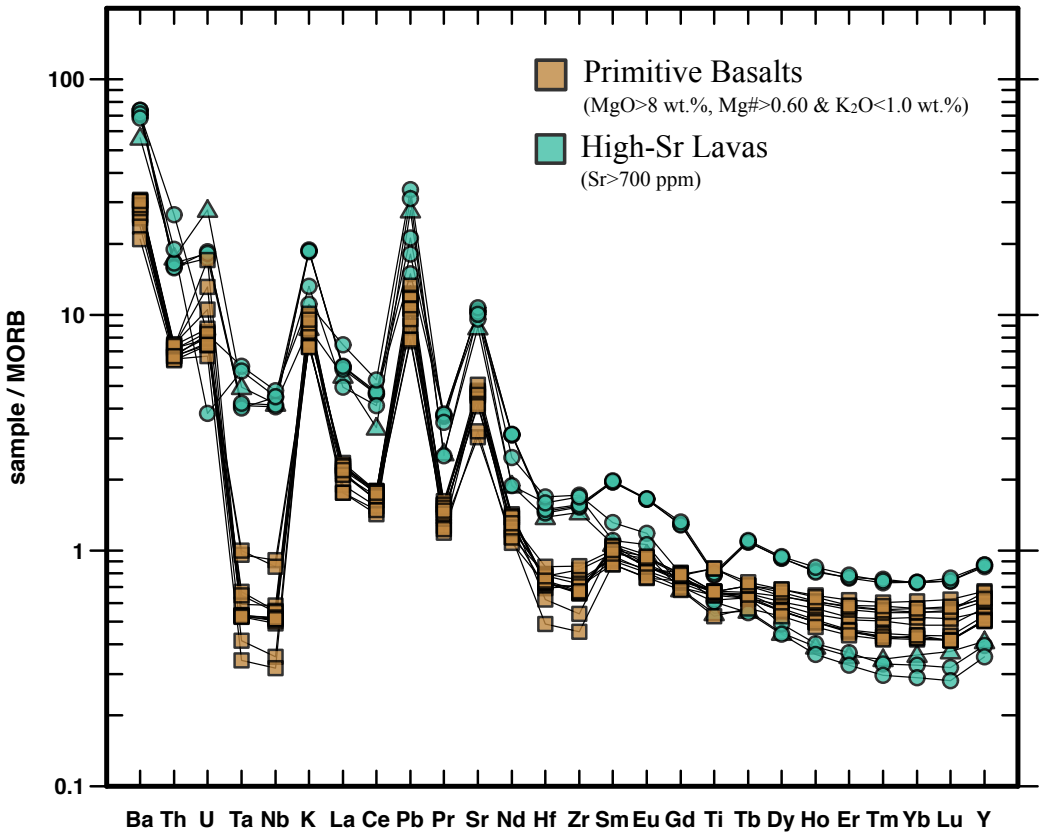

Figure 1.13. MORB-normalized incompatible element abundances for high-Sr lavas. Amber squares are as in Fig. 1.7. Teal symbols are as in Fig. 1.11C. Normalizing values are from Sun and McDonough (1989).

The few dacites present among the seafloor lavas have highly variable compositions. Dacites dredged from near Seguam Island (dredge #72) are evolved, with FeO*/MgO >4 and Mg#<0.30 (Fig. 1.6G). These samples have approximately 2 % K_2O and so fall in the center of the medium-K field at 70 % SiO_2 (Fig. 1.6C). Dacites dredged from an eroded cone near the Islands of Four Mountains (dredge #81) have more than 3.5 % K_2O. These rocks fall in the high-K field and are among the most potassic volcanic rocks in the arc (Fig. 1.6C). In contrast, dacites dredged from seafloor cones near Little Sitkin (dredges #33, #42) fall within or near the low-K field at 63-65 % SiO_2 (0.80-1.1 % K_2O). Both of these dacites fall in the calc-alkaline field, but one is highly calc-alkaline, with FeO/MgO<1 and Mg#=0.65 (Fig. 1.6G). Complete trace element data are available only for the dacites dredged near Seguam Island, mentioned above. Rare-earth elements for these are relatively flat, with high abundances for all REEs and well-defined negative Eu anomalies (Fig. 1.11B). These samples closely resemble dacitic lavas erupted on Seguam Island and studied by Singer et al. (1992).

Isotopic compositions for the seafloor lavas span nearly the full range of compositions observed in the Aleutians for the Pb, Sr, Nd and Hf systems. This variability is well expressed in the Nd-Sr isotope correlation diagram (Fig. 1.14A), in Pb-Pb isotope plots (Fig. 1.15A), and in plots of Sr versus Pb isotope (Fig. 1.15B). Few analyses are available for the Hf system, but there too, the seafloor lavas span most of the total range of compositions see in Aleutian lavas (Fig. 1.14B).

Most of the samples for which isotopic data are available are basalts, including several of both the low/med-K and the med/high-K primitive basalt types. It is evident that the med/high-K basalts have generally less radiogenic Pb and Sr than do the

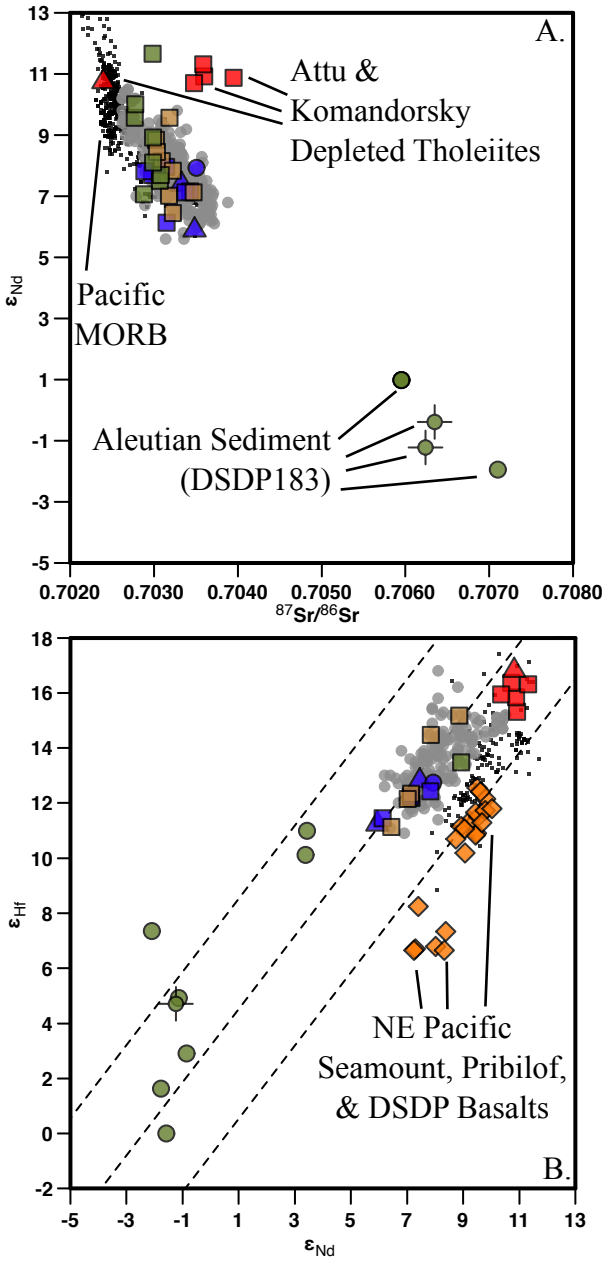

Figure 1.14. Neodymium-Sr (A) and Hf-Nd (B) isotope plots. Symbols are as in Fig. 1.6 with the addition of red symbols as Attu and Komandorsky depleted tholeiites, green circles as Aleutian sediments from DSDP site 183, black dots as Pacific MORB and orange diamonds as northeast Pacific seamount, Pribilof and DSDP 183 and 178 basalts. Dashed lines in B are after Vervoort and Blichert-Toft (1999). The center dashed line represents the Hf-Nd isotope mantle array and the other two dashed lines are ± 4 ε_{Hf} units.

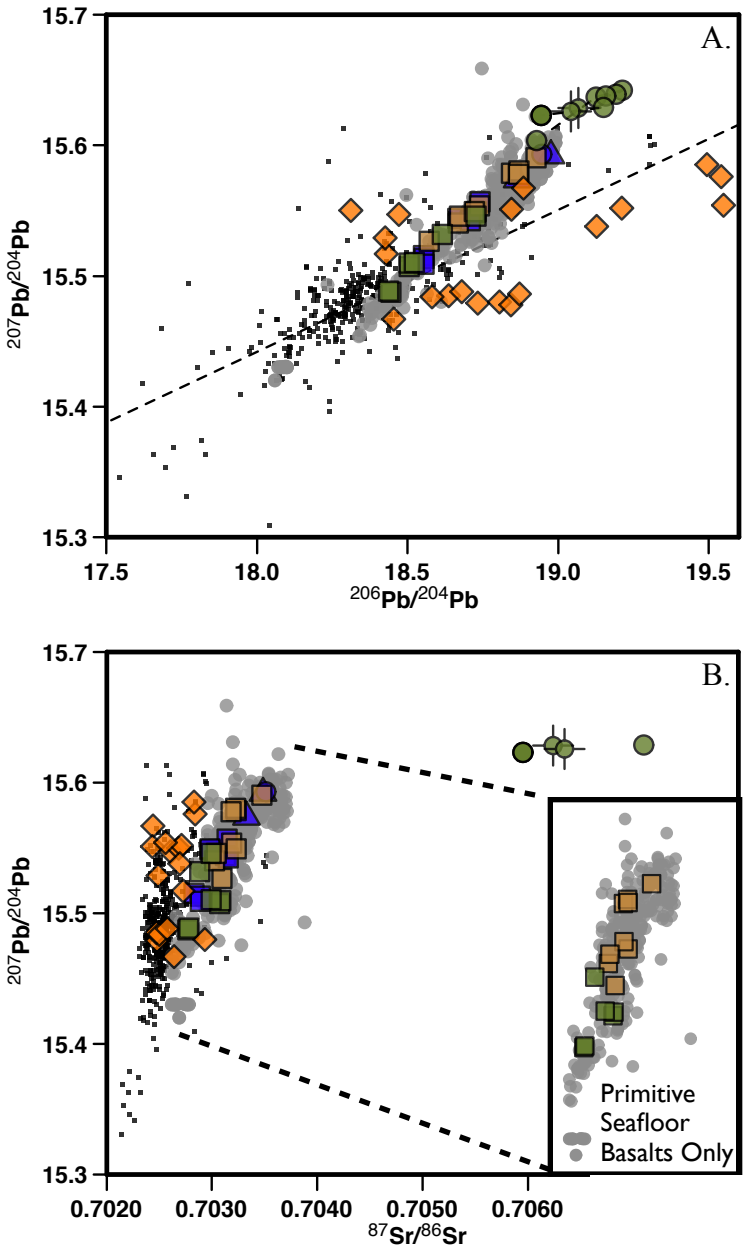

Figure 1.15. Lead isotope plot (A) and Pb-Sr isotope plot (B). Symbols are as in Fig. 1.14. Dashed line in 1.15A is the Northern Hemisphere Reference Line (NHRL). The inset in 1.15B is of primitive seafloor basalts only.

low/med-K primitive basalt types (Fig. 1.15B). These differences are evident for samples collected from widely separated locations, including both the western part of the study area near Little Sitkin and the eastern part of the study area near Seguam Island.

Along-arc changes in the isotopic compositions of Aleutian lavas have been well documented and are interpreted to reflect decreasing contributions of subducted marine sediment to the source of Aleutian lavas from east to west along the arc (Kelemen et al., 2003; Yogodzinski et al., 2010). These changes are also evident in seafloor lavas collected in locations spanning much of the eastern and central Aleutian arc length, from approximately 168°W to 178°E longitude (Fig. 1.1). Shifts toward MORB-like compositions in more westerly locations (reflecting less sediment in the source) are particularly clear for Pb and Sr isotopes (Fig. 1.16A, G). It also appears that at a given location in the arc, the seafloor lavas have on average, less radiogenic Pb and Sr, and more radiogenic Nd and Hf (Fig. 1.16A-D).

The isotopic compositions of three andesitic samples collected from locations in the eastern part of the study area near the Islands of Four Mountains (dredge #78, 83 and 85) are similar to those in the low/med-K basalt group, which are typical of lavas from easterly locations in the arc, with relatively radiogenic Pb and Sr, and relatively unradiogenic Nd and Hf (Fig. 1.16).

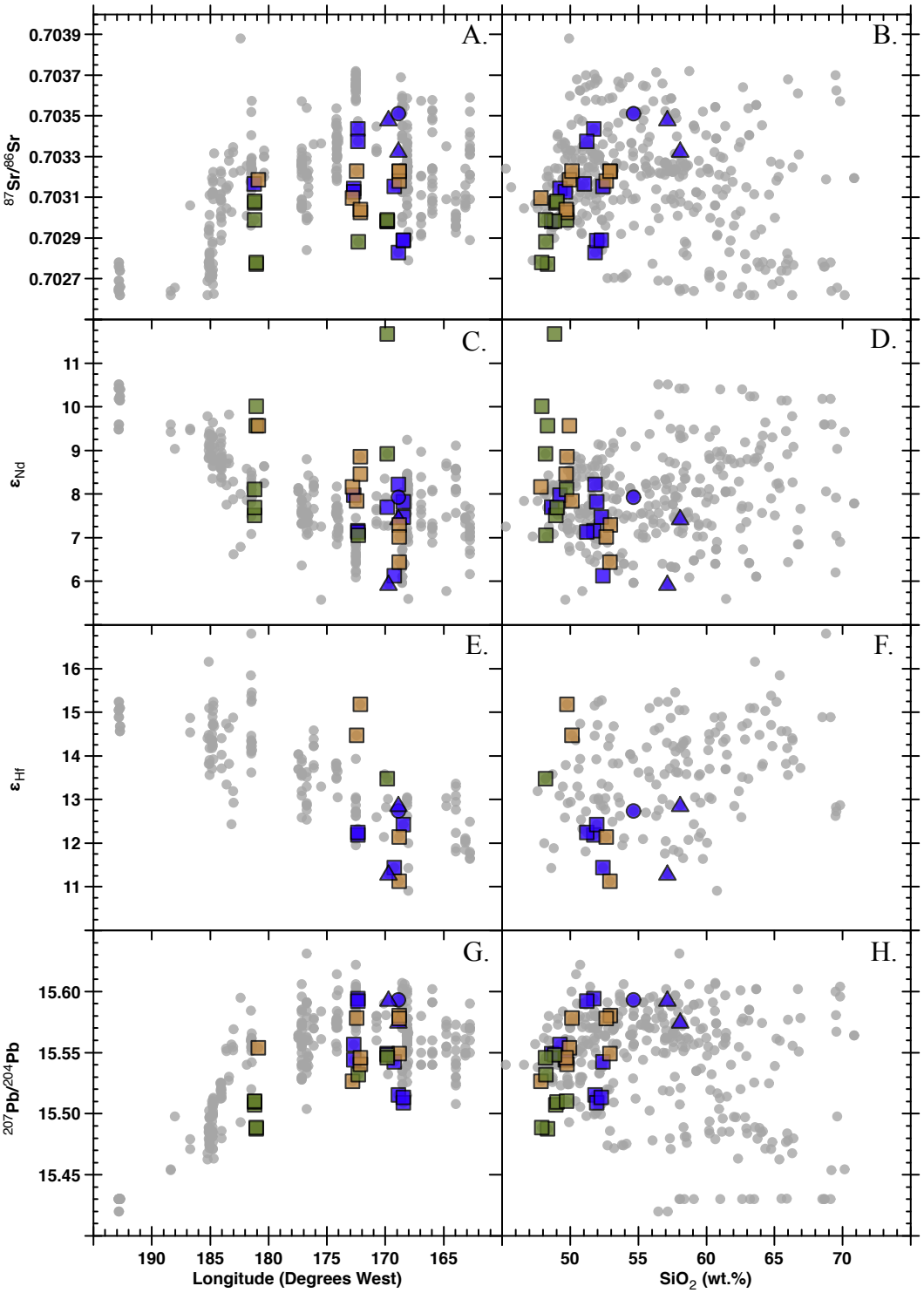

Figure 1.16. Harker diagrams of Sr, Nd, Hf and Pb isotopes as well as isotopes versus longitude in degrees west. Symbols are as in Fig. 1.6.

Chapter 2

Discussion and Conclusions

2.1 Overview of Central and Eastern Aleutian Seafloor Lavas

There are a relatively large number of primitive, high-Mg# compositions among the seafloor lavas (~30%). This is a high proportion of primitive lava compositions compared to sample sets from most Aleutian volcanoes. The distinctively primitive nature of the seafloor sample set is made clear by comparison with Little Sitkin and Korovin (two emergent volcanoes located in similar parts of the arc as the primitive seafloor lavas) where 153 samples include only two with Mg#s>0.60. Most primitive seafloor lavas are basalts, but a few have intermediate compositions with up to 64 % SiO_2.

Interestingly, all of the primitive seafloor lavas were dredged from volcanic features located at distances greater than approximately 18 km from the nearest large, emergent volcanic centers (Fig. 2.1). These lavas are likely to have experienced relatively little cooling and fractionation while ascending to the surface. This may be because the primitive seafloor lavas did not pass through the network of conduits and magma storage areas that underlie the major centers. These observations are consistent with the idea that small volume eruptions formed off the main volcanic axis may more accurately sample the geochemical heterogeneity that is present at depth (e.g., Lundstrom et al., 1999). The absence of primitive lavas from locations closer to the major centers could also indicate that the network of conduits and magma storage areas that underlie

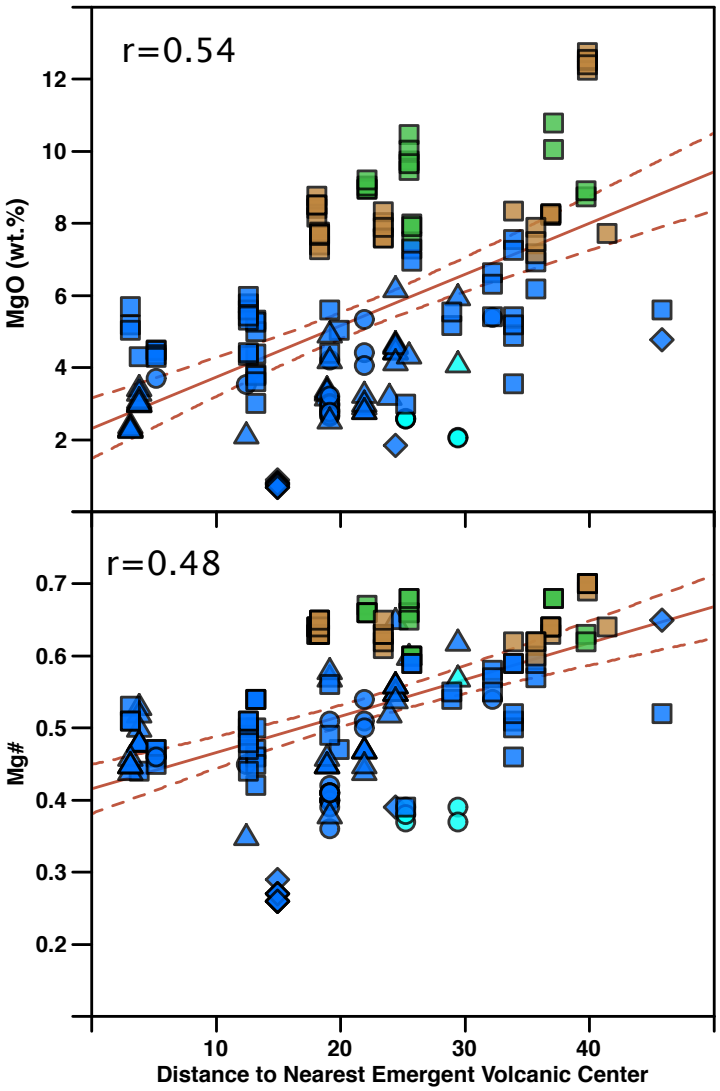

Figure 2.1. MgO and Mg# versus distance to the nearest emergent volcanic center. Symbols are as in Fig. 1.12. Solid red lines are least squares y on x regression lines calculated from the data and the dashed red lines represent the 95% confidence interval for the regression. Correlation coefficients (r) are displayed on each plot.

the major centers may have an effective footprint of 15-20 km. This would imply that magma storage areas beneath the major centers extend to at least this depth within the crust, and perhaps all the way to the crust-mantle boundary (e.g., Dahren et al., 2012).

Most of the evolved seafloor lavas in our data set are probably related to primitive seafloor basalts by fractional crystallization and mixing processes. These evolved lavas commonly have REE patterns parallel to primitive seafloor basalts but at higher REE abundances (Fig. 1.11). Evolved seafloor lavas with relatively steep REE patterns and higher K_2O concentrations (Fig. 1.11) may be related to med/high-K basalts by fractional crystallization. Many of the evolved seafloor andesites have REE patterns with suppressed middle REE abundances compared heavy REEs (low Dy/Yb; Fig. 1.11B). Romick et al. (1992) and Davidson et al. (2007) show that these trace element characteristics are common in arc andesites and dacites, and they argue that it is produced primarily by a fractionating mineral assemblage that includes amphibole. Observations of hand specimens confirm that amphibole is a prominent phenocryst mineral in all of the seafloor andesites that have relatively low middle and heavy REE abundances, and relatively low Dy/Yb.

High-Sr lavas with strongly fractionated REE patterns (Fig. 1.11C) are unlikely to be related to primitive basalts by fractional crystallization and mixing processes. The very steep REE patterns of these lavas indicate a significant role for garnet in their formation. The high-Sr lavas with strongly fractionated REE patterns are depleted in Yb compared to Dy, similar to dacites among the western Aleutian seafloor lavas. These are the characteristics of the Adak and Komandorsky magnesian andesites (adakites), which are isotopically similar to MORB, and are interpreted to have been formed in a multi-

stage process that includes a significant role for partial melting of subducted oceanic crust in the presence of garnet (Kay, 1978; Yogodzinski et al., 1995; Kelemen et al., 2003).

The Adak and Komandorsky magnesian andesites have relatively high La and Ce, but low Ta and Nb, and so based on La/Ta and La/Nb ratios, are the most Ta-Nb-depleted lavas in the Aleutian arc (Yogodzinski et al., 1995). By comparison, several of the high-Sr seafloor lavas also have elevated La and Ce, but their Ta and Nb abundances are also elevated, so their La/Ta and La/Nb ratios are close to those of MORB.

It is generally agreed that Ta and Nb depletions reflect a role for residual rutile in the source of arc lavas (e.g., Weyer et al., 2003). Experimental studies by Klemme et al. (2002) show that the stability of rutile in the subducting slab is controlled by temperature, degree of partial melting and bulk composition of the slab. In general, the effect of increasing temperature in magmatic systems is to increase the solubility of accessory minerals such rutile (Klemme et al., 2002; Klimm et al., 2008). Assuming that residual rutile in arc systems is stabilized during partial melting of eclogite, the effect of increasing temperature will be to increase the abundance of Nb and Ta in the melt. This is due to the increased solubility of rutile at higher temperatures, which decreases the amount of rutile present in the system. As temperature increases, the concentration of Nb and Ta in the melt equilibrated with rutile will also increase, up to the point where rutile is eliminated from the residue. At that temperature, Nb and Ta abundances will be at their highest concentrations, and will decrease progressively by dilution if the temperature and degree of melting continue to increase (Klemme et al., 2002; Klimm et al., 2008). High-Sr seafloor lavas with La/Ta and La/Nb ratios close to MORB may

indicate Nb and Ta were eradicated from the subducting slab in the back arc due to an increase in the temperature of the slab causing the solubility of rutile to increase, specifically beneath the cones where these lavas were collected.

2.2 Origin of Med/High-K Back-Arc Basalts

Geochemical characteristics like those seen in med/high-K Aleutian seafloor basalts have been observed in subduction back arc settings worldwide, and present a classic problem of subduction-related magma genesis (Barth, 1956; Byers, 1961; Dickinson and Hatherton, 1967; Hochstaedter et al., 2001; Hildreth et al., 2004; Stern et al., 2006; Tollstrup et al., 2010; Watt, 2013). Back-arc lavas of this type, which are generally recognized by their higher K_2O concentrations compared to similarly evolved volcanic front lavas, have been broadly attributed to the location on the overriding plate relative to the trench or volcanic front, and/or to the depth to the underlying subducting plate. Barth (1956) observed higher K_2O in lavas from the Pribilof Islands in the Bering Sea compared to lavas of the Aleutian volcanic front. He suggested that this was due to crustal instability and vertical faulting in the vicinity of the Pribilof Islands. Similarly, Byers (1961) considers tension fractures in the Aleutian back arc oriented normal to the arc as an explanation for higher K_2O concentrations in Bogoslof lavas compared to lavas from Umnak Island located on the volcanic front. Arculus et al. (1977) found Sr isotopes of Bogoslof lavas to be relatively unradiogenic compared to Umnak lavas, and they suggested this was due to parental melts being of mantle origin. Dickinson and Hatherton (1967) were the first to document cross-arc increasing K_2O concentrations with increasing vertical depth to the Benioff zone as a global phenomenon. They suggested that elevated K_2O in back-arc lavas arose at the sites of initial partial melting

along the Benioff zone, and emphasized that the melts experienced relatively little change in K_2O as they rose to the surface.

Hildreth et al. (2004) found that back arc lavas from the Katmai reach of the Alaska Peninsula have relatively high K_2O concentrations, are more enriched in light REEs (high La/Yb) and have less radiogenic Sr compared to volcanic front lavas. They interpret the relative enrichment of K_2O and light REEs in back arc lavas to result from lower degrees of mantle melting compared to volcanic front lavas. Radiogenic Sr in volcanic front lavas is suggested by Hildreth et al. (2004) to be in part caused by higher slab flux beneath the volcanic front. Hildreth et al. (2001) also note that a correlation of Sr isotopes with indices of fractionation in volcanic front lavas indicates a significant role for crustal contributions and concludes that less radiogenic Sr in rear arc lavas is due to a lesser crustal influence.

Watt (2013) has also observed higher K_2O and relative enrichment of light REEs in high MgO melt inclusions hosted in olive in back arc lavas from southern Chile. He too suggests that lower degrees of mantle melting produce the enrichments of these elements in the back arc lavas. Watt (2013) also speculates that addition of a melt derived from subducted oceanic crust to the overlying mantle wedge beneath the back arc, could also increase K_2O and light REE abundances in back arc lavas.

The Izu-Bonin-Mariana arc (IBM) system, basalts produced in seamount chains behind that main volcanic front are less radiogenic in all isotope systems (Sr, Nd, Hf and Pb) compared to volcanic front basalts (Tollstrup et al., 2010; Hochstaedter et al., 2001; Stern et al., 2006). This is usually interpreted to reflect heterogeneity in the Indian-type mantle wedge (Pb isotopes plot above the NHRL) and the presence of components from

subducted Indian-type sediment and Pacific-type altered oceanic crust (Pb isotopes plot below the NHRL), which are added to the mantle in different proportions (Tollstrup et al., 2010; Hochstaedter et al., 2001). Stern et al. (2006) argues that IBM back-arc basalts have less radiogenic Sr because there is less subducted sediment and altered oceanic crust beneath the back arc. All of these author interpret higher K_2O and light REEs in back arc basalts as a result of lower degrees of mantle melting compared to volcanic front lavas and/or the presence of geochemically enriched Indian-type mantle (Tollstrup et al., 2010; Hochstaedter et al., 2001; Stern et al., 2006).

In Aleutian back arc basalts, we observe enrichments in nearly all incompatible elements relative to Pb (Fig. 1.8) coupled to generally less radiogenic Pb and Sr isotopes (Fig. 2.2). This produces clear inverse relationships between Pb isotopes and abundance ratios for a variety of trace elements relative to Pb (Fig. 2.2). These coupled isotope-trace element systematics may be explained primarily by a decreased role in the source for subducted sediment, which is an abundant source of Pb (12-14 ppm in average Aleutian sediment – Vervoort et al., 2011) that is also exceptionally radiogenic ($^{207}Pb/^{204}Pb$~15.626).

Contributions of the subducted sediment and other source components can be modeled based on data patterns in a graph of $^{207}Pb/^{204}Pb$ versus Ce/Pb (Fig. 2.3). Miller et al. (1994) showed that geochemical source components are located in widely separated corners on this plot. Two components with relatively unradiogenic Pb are separated widely based on Ce/Pb, which is relatively high in the MORB or depleted mantle component, compared to fluids and/or melts of subducted basalt, which have low Ce/Pb (Fig. 2.3). The component with radiogenic Pb and low Ce/Pb is subducted sediment.

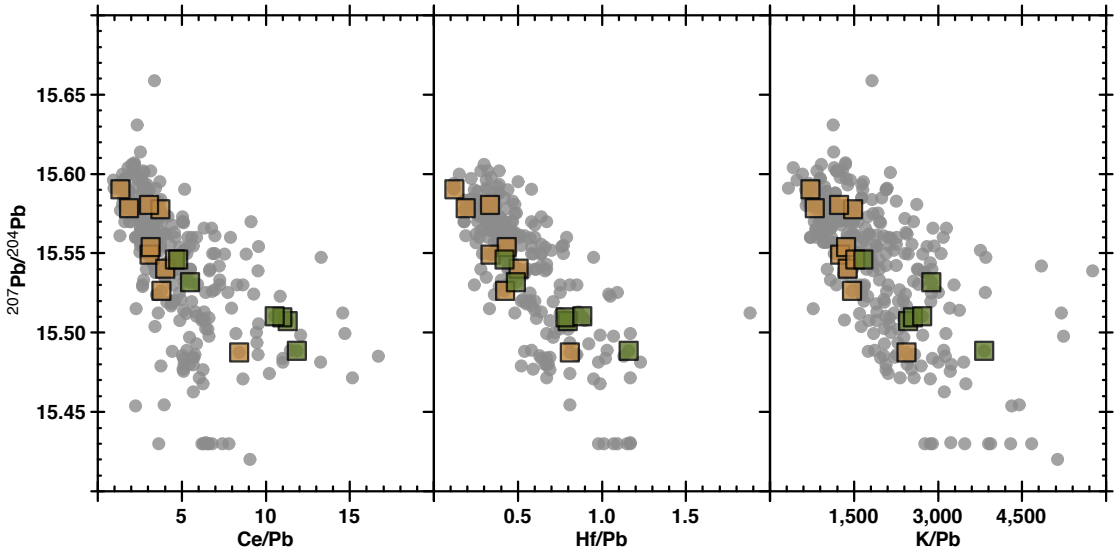

Figure 2.2. Lead isotopes versus incompatible elements relative to Pb. Symbols are as in Fig. 1.6.

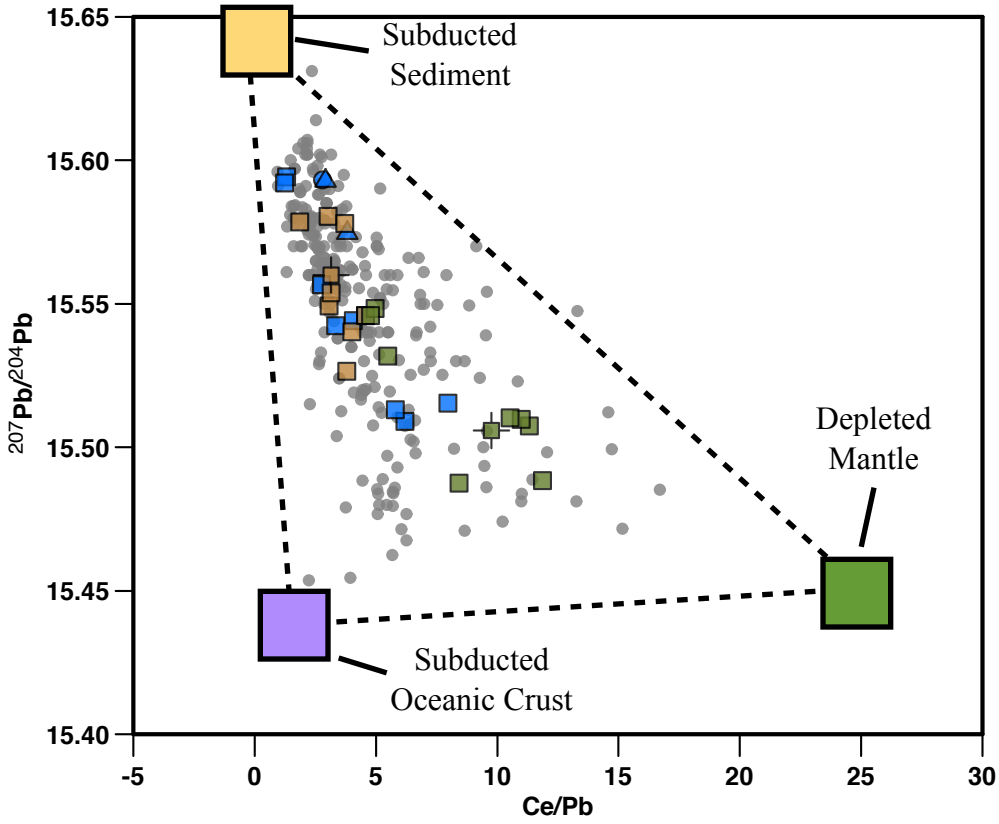

Figure 2.3. Lead isotopes versus Ce/Pb. Adapted from Miller et al. (1994). Source components are labeled and represented by colored squares. Dashed lines are mixing lines between source components. Symbols are as in Fig. 1.6 with the addition of green and brown squares with crosshairs for med/high-K basalt and low/med-K basalt averages, respectively.

Because mixing lines on this graph are straight, the location of each data point represents a unique combination of the three end-members, which define the vertices of the scalene triangle (Fig. 2.3).

Source contributions were calculated from this three-component system for each of the primitive back-arc basalts and for average low/med-K and med/high-K groups. End-member compositions for the system are defined by assigning $^{207}Pb/^{204}Pb$ and Ce/Pb compositions that encompass most Aleutian lavas (Fig. 2.3). Because the end-members are widely spaced on the graph, the selection of slightly different end-member compositions has relatively little effect on the outcome of the calculation. The calculations indicate that Ce and Pb in the average primitive low/med-K basalt are contributed predominantly by subducted sediment (62%), with significantly lower contributions for these elements from subducted basalt (29%) and depleted mantle (9%). For the average med/high-K primitive basalt, all three components contribute equally to the source for Ce and Pb. This reflects the fact that the average med/high-K primitive basalt falls nearly at the center of the triangular region outlined in Fig. 2.3.

These results are not subject to assumptions about the concentrations of Pb or Ce in the end-members. They reflect only the positions of the data points relative to the corners of the triangle. This means in turn, that the calculations provide no information about the abundances of Ce and Pb in lavas. The results are qualitatively consistent with the general pattern of decreasing abundances of K, Ce, Hf and other incompatible elements relative to Pb with decreasing $^{207}Pb/^{204}Pb$ and $^{87}Sr/^{86}Sr$ (Fig. 2.2), because the component that is reduced the most in the med/high-K basalts is the subducted sediment, which has high concentrations of Pb (12-14 ppm – Vervoort et al., 2011). Interpretations

about the concentrations of these elements in the primitive basalts, will require additional modeling with assumptions about the abundances of Ce, Pb and other trace elements in the aqueous fluids or hydrous partial melts that were produced when these elements were extracted from subducted sediment and basalt (e.g., Kessel et al., 2005). One thing that seems clear is that relatively high abundances of incompatible elements in the med/high-K basalts will not be explained only by shifting proportions of the source components. This is true because the depleted mantle component is expected to be the least fertile source of incompatible elements, and because it is the one component that is present in significantly higher proportion in the med/high-K basalts (34%) compared to the low/med-K basalts (9%). It therefore seems likely that some other process, perhaps a lower degree of mantle melting, has contributed to the higher concentrations of incompatible elements in the med/high-K basalts.

2.3 Characterizing the Aleutian Mantle

Because the med/high-K back-arc basalts were produced from a source mixture with significantly less sediment and more of the mantle component than is typical for Aleutian volcanic rocks (Fig. 2.3), they provide an opportunity to better-characterize the geochemical nature of the Aleutian mantle wedge, as it exists prior to mixing with subducted components. This is a key issue because if the sub-arc mantle is enriched or plume-influenced, or if it is a plumb pudding of enriched and depleted components, then melting of the mantle component may produce ocean-island type basalts, which display many of the same trace element enrichments as those seen in arc magmas, but without any immediate role for subduction-recycling. This issue has been discussed at length (Morris & Hart, 1983; Perfit & Kay, 1986). The major issues were mostly resolved by

^{10}Be studies, which showed that subduction recycling of ocean floor sediment plays a significant role in controlling the compositions of most island-arc volcanic rocks (Morris et al., 1990; Monoghan et al., 1988; Tera et al., 1986). However the issue resurfaces, especially when there is an effort to calculate elemental budgets for arc magmas or recycling rates, which depend heavily on assumptions about mantle contributions during magma genesis (Plank, 2005; Singer et al., 2007).

The broad isotopic patterns for all Aleutian lavas, especially those of med/high-K basalts, appear inconsistent with the involvement of an enriched mantle or plume component in the Aleutian back-arc. Aleutian lavas, including one of the med/high-K basalts, plot along the center of the mantle array for Hf-Nd isotopes, while apparently plume-influenced basalts, including DSDP 183 and 178 basement basalts, and northeast Pacific seamounts, all have higher ε_{Nd} at similar ε_{Hf} (Fig. 1.14B). Basalts from the Pribilof Islands (Fig. 1.1) also fall in this field and are interpreted to have been formed by recent enrichment of the upper mantle beneath the continental margin (Chang et al., 2009), but an enriched plume source is considered to cause the isotopic compositions of northeast Pacific seamounts (Chadwick et al., 2013). The med/high-K basalts also plot inline with the Aleutian array, which trends toward less radiogenic Pb and Sr (Fig. 1.15B). Some northeast Pacific seamounts have unradiogenic Sr, but when compared to med/high-K basalts, they have more radiogenic Pb at similar Sr isotopic compositions. In $^{207}Pb/^{204}Pb$-$^{206}Pb/^{204}Pb$ space (Fig. 1.15A), med/high-K basalts again plot along the Aleutian array toward unradiogenic values. Northeast Pacific plume basalts are highly variable on this plot, but the likelihood of the involvement of an enriched mantle source in the production of med/high-K basalts is low compared to the more simple explanation

of a depleted mantle source. Additional isotopic measurements for Hf will have to be made on Aleutian back-arc basalts before the nature of their mantle source can be confidently established.

2.4 Conclusions

Mapping and dredging of small volcanic cones located between and behind the emergent volcanoes of the Aleutian arc has led to the discovery of primitive med/high-K basalts in the Aleutian back-arc. Lavas with comparable geochemistry have not been previously observed in emergent volcanoes of the Aleutian arc.

Modeling of source component contributions based on data patterns in $^{207}Pb/^{204}Pb$-Ce/Pb space indicate that there is an increased role for depleted mantle and a decreased role for subducted sediment in the source of Aleutian back-arc lavas. The average low/med-K basalt, which is analogous to common Aleutian primitive basalts, obtains Ce and Pb predominantly from subducted sediment (62%), with notably lower contributions from subducted basalts (29%) and depleted mantle (9%). In contrast, model calculations indicate all three components contribute Ce and Pb equally to the average med/high-K basalt.

A role for relatively low-degree melting in the creation of the med/high-K basalts seems likely but has not been quantified. Medium/high-K basalts are produced with relatively greater contributions from the depleted mantle and have higher abundances of incompatible elements, however, the depleted mantle is the least fertile source of incompatible elements. Modeling of low-degree melting to produce med/high-K basalts may resolve this issue.

Isotopic shifts in the med/high-K basalts indicate that the Aleutian sub-arc mantle is depleted (MORB-like), not enriched. Medium/high-K basalts plot along the Aleutian array on Pb, Sr, Nd and Hf isotope variation diagrams, which trends toward unradiogenic Pb and Sr and radiogenic Nd and Hf. The Aleutian array plots along the mantle array in Hf-Nd isotope space. Analyzing Hf isotopes for the remaining med/high-K basalts will likely strengthen this argument.

References

Arculus, R.J., Delong, S.E., Kay, R.W., Brooks, C., and Sun, S.S., 1977, The alkali rock suite of Bogoslof Island, eastern Aleutian arc, Alaska: Journal of Geology, v. 85, p. 177-186.

Barth, T.F.W., 1956, Geology and petrology of the Pribilof Islands, Alaska: U.S. Geological Survey Bulletin, 1028-F, p. 101-160.

Byers, F.M., 1961, Petrology of three volcanic suites, Umnak and Bogoslof Islands, Aleutian Islands, Alaska: Geological Society of America Bulletin, v. 72, p. 93-128.

Chadwick, J., Keller, R. A., Kamenov, G., Yogodzinski, G. M., and Lupton, J., 2013, Progressive Compositional Changes in Cobb Hotspot Lavas: Effects of Juan de Fuca Ridge Convergence and a Thinning Lithospheric Lid: (manuscript in preparation).

Chang, J. M., Feeley, T. C., and Deraps, M. R., 2009, Petrogenesis of basaltic volcanic rocks from the Pribilof Islands, Alaska, by melting of metasomatically enriched depleted lithosphere, crystallization differentiation, and magma mixing: Journal of Petrology, v. 50, p. 2249-2286.

Dahren, B., Troll, V. R., Andersson, U. B., Chadwick, J. P., Gardner, M. F., Jaxybulatov, K., and Koulakov, I., 2012, Magma plumbing beneath Anak Krakatau volcano, Indonesia: evidence for multiple magma storage regions: Contributions to Mineralogy and Petrology, v. 163, p. 631-651.

Davidson, J., Turner, S., Handely, H., Macpherson, C., and Dosseto, A., 2007, Amphibole "sponge" in arc crust?: Geology, v. 35, p. 787-790.

Dickinson, W.R., and Hatherton, T., 1967, Andesitic volcanism and seismicity around the Pacific: Science, v. 157, p. 801-803.

Elliott, T., Plank, T., Zindler, A., White, W., and Bourdon, B., 1997, Element transport from slab volcanic front at the Mariana arc: Journal of Geophysical Research, v. 102, p. 14,991-15,019.

Gill, J., 1981, Orogenic Andesites and Plate Tectonics: New York, Springer-Verlag, 390 p.

Gust, D. A., and Perfit, M. R., 1987, Phase relations of a high-Mg basalt from the Aleutian Island arc: implications for primary island arc basalts and high-Al basalts: Contributions to Mineralogy and Petrology, v. 97, p. 7-18.

Hawkesworth, C.J., Gallagher, K., Hergt, J.M., and McDermott, F., 1993, Mantle and slab contributions in arc magmas: Annual Review of Earth and Planetary Science, v. 21, p. 175-204.

Hildreth, W., Fierstein, J., Siems, D.F., Budahn, J.R., and Ruíz, J., 2004, Rear-arc vs. arc-front volcanoes in the Katmai reach of the Alaska Peninsula: a critical appraisal of across-arc compositional variation: Contributions to Mineral Petrology, v. 147, p. 243-275.

Hochstaedter, A., Gill, J., Peters, R., Broughton, P., Holden, P., and Taylor, B., 2001, Across-arc geochemical trends in the Izu-Bonin arc: Contributions from the subducting slab: Geochemistry Geophysics Geosystems, v. 2.

Jicha, B. R., Scholl, D. W., B.S., S., Yogodzinski, G. M., and Kay, S. M., 2005, Revised 40Ar/39Ar age of Aleutian island arc formation implies high rate of magma production: Eos - Transactions of the American Geophysical Union, v. 86(52) Fall Meeting Supplement, p. Abstract V51D-1514.

Johnson, D. M., Hooper, P. R., and Conrey, R. M., 1999, XRF analysis of rocks and minerals for major and trace elements on a single low dilution Li-tetraborate fused bead: Advances in X-ray Analysis, v. 41, p. 843-867.

Kay, R.W., 1978, Aleutian magnesian andesites: Melts from subducted Pacific oceanic crust: Journal of Volcanology and Geothermal Research, v. 4, p. 117-132.

Kay, R.W., 1980, Volcanic arc magma genesis: implications for element recycling in the crust-upper mantle system: Journal of Geology, v. 88, p. 497-522.

Kay, S. M., and Kay, R. W., 1994, Aleutian Magmas in Space and Time, in Plafker, G., and Berg, H. C., eds., The Geology of Alaska. The Geology of North America, v. G-1: Boulder, Geological Society of America, p. 687-722.

Kelemen, P. B., Yogodzinski, G. M., and Scholl, D. W., 2003, Along-strike variation in lavas of the Aleutian Island Arc: Implications for the genesis of high Mg# andesite and the continental crust, in Eiler, J., ed., Inside the Subduction Factory, Geophysical Monograph 138: Washington D.C., American Geophysical Union, p. 223-276.

Kelley, K. A., Plank, T., Ludden, J. N., and Staudigel, H., 2003, Composition of altered oceanic crust at ODP Sites 801 and 1149: Geochemistry Geophysics Geosystems, v. 4, p. 21.

Kessel, R., Schmidt, M.W., Ulmer, P., and Pettke, T., 2005, Trace element signature of subduction-zone fluids, melts and supercritical liquids at 120-180 km depth: Nature, v. 437, p. 724-727.

Klemme, S., Blundy, J. D., and Wood, B.J., 2002, Experimental constraints on major and trace element partitioning during partial melting of eclogite: Geochimica et Cosmochimica Acta, v. 66, p. 3109-3123

Klimm, K., Blundy, J. D., and Green, T. H., 2008, Trace element partitioning and accessory phase saturation during H2O-Saturated melting of basalt with implications for subduction zone chemical fluxes: Journal of Petrology, v. 49, p. 523-553.

Krogh, T.E., 1973, A low-contamination method for hydrothermal decomposition of zircon and extraction of U and Pb for isotopic age determinations: Geochimica et Cosmochimica Acta, v. 37, p. 485-494.

Lugmair, G. W., and Carlson, R. W., 1978, The Sm-Nd history of KREEP: Proceedings of the 9th Lunar Planetary Science Conference, p. 689-704.

Lundstrom, C. C., Sampson, D. E., Perfit, M. R., Gill, J., and Williams, Q., 1999, Insights into mid-ocean ridge basalt petrogenesis: U-series disequilibria from the Siqueiros Transform, Lamont Seamounts, and East Pacific Rise: Journal of Geophysical Research, v. 104, p. 13,035-13,048.

McDonough, W.F., and Sun, S.S., 1995, The composition of the earth: Chemical Geology, v. 120, p. 223-253.

Miller, D.M., Goldstein, S.L., and Langmuir, C.H., 1994, Cerium/lead and lead isotope ratios in arc magmas and the enrichment of lead in the continents: Nature, v. 368, p. 514-519.

Miyashiro, A., 1974, Volcanic rock series in island arcs and active continental margins: American Journal of Science, v. 274, p. 321-355.

Monaghan, M. C., Klein, J., and Measures, C. I., 1988, The origin of ^{10}Be in island-arc volcanic rocks: Earth and Planetary Science Letters, v. 89, p. 288-298.

Monaghan, M., Measures, C., Klein, J., and Middleton, R., 1987, ^{10}Be and ^{9}Be in phenocryst and groundmass separates from Aleutian-arc volcanic rocks: implications for a magmatic origin of ^{10}Be in island-arc lavas: Transactions American Geophysical Union, v. 68, p. 1525.

Morris, J. D., and Hart, S. R., 1983, Isotopic and incompatible trace element constraints on the genesis of island arc volcanics from Cold Bay and Amak Island, Aleutians, and implications for mantle structure: Geochimica et Cosmochimica Acta, v. 47, p. 2015-2030.

Morris, J.D., Leeman, W.P., and Tera, F., 1990, The subduction component in island arc lavas: constraints from Be isotopes and B-Be systematics: Nature, v. 344, p. 31-35.

Nye, C. J., and Reid, M. R., 1986, Geochemistry of primary and least fractionated lavas from Okmok Volcano, central Aleutians: Implications for Arc magma genesis: Journal of Geophysical Research, v. 91, p. 10271-10287.

Perfit, M. R., and Kay, R. W., 1986, Comment on isotopic and incompatible element constraints on the genesis of island arc volcanics from Cold Bay and Amak Island, Aleutians, and implications for mantle structure: Geochimica et Cosmochimica Acta, v. 50, p. 477-481.

Plank, T., 2005, Constraints from Thorium/Lanthanum on sediment recycling at subduction zones and the evolution of continents: Journal of Petrology, v. 46, p. 921-944.

Plank, T., and Langmuir, C.H., 1993, Trace elements from sediment input to volcanic output at subduction zones: Nature, v. 362, p. 739-742.

Romick, J. D., Kay, S. M., and Kay, R. W., 1992, The influence of amphibole fractionation on the evolution of calc-alkaline andesite and dacite tephra from the central Aleutians, Alaska: Contributions to Mineralogy and Petrology, v. 112, p. 101-118.

Singer, B., Jicha, B. R., Leeman, W. P., Rogers, N. W., Thirlwall, M. F., Ryan, J., and Nicolaysen, K. E., 2007, Along-strike trace element and isotopic variation in Aleutian island arc basalt: subduction melts sediments and dehydrates serpentine: Journal of Geophysical Research, v. 112, p. B06206.

Singer, B. S., Myers, J. D., and Frost, C. D., 1992, Mid-Pleistocene lavas from the Seguam Island volcanic center, central Aleutian arc: Closed-system fractional crystallization of a basalt to rhyodacite eruptive suite: Contributions to Mineralogy and Petrology, v. 110, p. 87-112.

Stern, R.J., Kohut, E., Bloomer, S.H., Leybourne, M., Fouch, M., and Vervoort, J., 2006, Subduction factory processes beneath the Guguan cross-chain, Mariana Arc: no role for sediments, are serpentinites important?: Contributions to Mineral Petrology, v. 151, p. 202-221.

Sun, S.S., and McDonough, W.F., 1989, Chemical and isotopic systematics of oceanic basalts: implications for mantle composition and processes: Geological Society, London, Special Publications, v. 42, p. 313-345.

Tera, F., Brown, L., Morris, J. D., and Sacks, I. S., 1986, Sediment incorporation in island-arc magmas: Inferences from 10Be: Geochimica et Cosmochimica Acta, v. 50, p. 535-550.

Todt, W., Clift, R. A., Hanser, A., and Hofmann, A. W., 1996, Evaluation of a 202Pb-205Pb double spike for high precision lead analysis, *in* Basu, A., and Hart, S. R., eds., Earth processes: Reading the Isotopic Code: Geophysical Monograph 95: Washington, DC, Am. Geophys. Union, p. 429-437.

Tollstrup, D., Gill, J., Kent, A., Prinkey, D., Williams, R., Tamura, Y., and Ishizuka, O., 2010, Across-arc geochemical trends in the Izu-Bonin arc: Contributions from the subducting slab, revisited: Geochemistry Geophysics Geosystems, v. 11.

Vervoort, J.D., and Blichert-Toft, J., 1999, Evolution of the depleted mantle; Hf isotope evidence from juvenile rocks through time: Geochimica et Cosmochimica Acta, v. 63, p. 533-556.

Vervoort, J. D., Plank, T., and Prytulak, J., 2011, The Hf-Nd isotopic composition of marine sediments: Geochimica et Cosmochimica Acta, v. 75, p. 5903-5926.

Watt, S.F., Pyle, D.M., Mather, T.A., and Naranjo, J.A., 2013, Arc magma compositions controlled by linked thermal and chemical gradients above the subducting slab: Geophysical Research Letters, v. 40, p. 2550-2556

Weyer, S., Münker, C., and Mezger, K., 2003, Nb/Ta, Zr/Hf and REE in the depleted mantle: implications for the differentiation history of the crust-mantle system: Earth and Planetary Science Letters, v. 205, p. 309-324.

White, W. M., Albarède, F., and Télouk, P., 2000, High-precision analysis of Pb isotope ratios using multi-collector ICP-MS: Chemical Geology, v. 167, p. 257-270.

Yogodzinski, G.M., Kay, R.W., Volynets, O.N., Koloskov, A.V., and Kay, S.M., 1995, Magnesian andesite in the western Aleutian Komandorsky region: implications for slab melting and processes in the mantle wedge: Geological Society of America Bulletin, v. 107, p. 505-519.

Yogodzinski, G. M., Vervoort, J. D., Brown, S. T., and Gerseny, M., 2010, Subduction controls of Hf and Nd isotopes in lavas of the Aleutian island arc: Earth and Planetary Science Letters, v. 300, p. 226-238.

Yogodzinski, G.M., Volynets, O.N., Koloskov, A.V., Seliverstov, N.I., and Matvenkov, V.V., 1994, Magnesian andesites and the subduction component in a strongly calc-alkaline series at Piip Volcano, far western Aleutians: Journal of Petrology, v. 35, p. 163-204.